NASA Technical Memorandum 106831
AIAA–95–0755

Collection Efficiency and Ice Accretion Calculations for a Sphere, a Swept MS(1)-317 Wing, a Swept NACA-0012 Wing Tip, an Axisymmetric Inlet, and a Boeing 737-300 Inlet

C.S. Bidwell
National Aeronautics and Space Administration
Lewis Research Center
Cleveland, Ohio

and

S.R. Mohler, Jr.
NYMA, Inc.
Engineering Services Division
Brook Park, Ohio

Prepared for the
33rd Aerospace Sciences Meeting and Exhibit
sponsored by the American Institute of Aeronautics and Astronautics
Reno, Nevada, January 9–12, 1995

National Aeronautics and
Space Administration

Collection Efficiency and Ice Accretion Calculations for a Sphere, a Swept MS(1)-317 Wing, a Swept NACA-0012 Wing Tip, an Axisymmetric Inlet, and a Boeing 737-300 Inlet

C. S. Bidwell
National Aeronautics and Space Administration
Lewis Research Center
Cleveland, Ohio 44135

and

Stanley R. Mohler, Jr.
NYMA, Inc.
Engineering Services Division
Brook Park, Ohio 44142

ABSTRACT

Collection efficiency and ice accretion calculations have been made for a sphere, a swept MS(1)-317 wing, a swept NACA-0012 wing tip, an axisymmetric inlet, and a Boeing 737-300 inlet using the NPARC flow solver and the NASA Lewis LEWICE3D grid based ice accretion code. Euler flow solutions for the geometries were generated using the NPARC flow solver. The LEWICE3D grid based ice accretion program was used to calculate the impingement efficiencies and ice shapes. Ice shapes typifying rime and mixed icing conditions were generated for a 30 minute hold condition. All calculations were performed on an SGI Model Power Challenge Ccomputer. The results have been compared to experimental flow and impingement data. In general, the calculated flow and collection efficiencies compared well with experiment, and the ice shapes looked reasonable and appeared representative of the rime and mixed icing conditions for which they were calculated.

Collection Efficiency and Ice Accretion Calculations for a Sphere, a Swept MS(1)-317 Wing, a Swept NACA-0012 Wing Tip, an Axisymmetric Inlet, and a Boeing 737-300 Inlet

Colin S. Bidwell
National Aeronautics and Space Administration
Lewis Research Center
Cleveland, Ohio 44135

and

Stanley R. Mohler, Jr.
NYMA, Inc.
Engineering Services Division
Brook Park, Ohio 44142

SUMMARY

Collection efficiency and ice accretion calculations have been made for a sphere, a swept MS(1)-317 wing, a swept NACA-0012 wing tip, an axisymmetric inlet, and a Boeing 737-300 inlet using the NPARC flow solver and the NASA Lewis LEWICE3D grid based ice accretion code. Euler flow solutions for the geometries were generated using the NPARC flow solver. The LEWICE3D grid based ice accretion program was used to calculate impingement efficiency and ice shapes. Ice shapes typifying rime and mixed icing conditions were generated for a 30 minute hold condition. All calculations were performed on an SGI Power Challenge computer. The results have been compared to experimental flow and impingement data. In general, the calculated flow and collection efficiencies compared well with experiment, and the ice shapes looked reasonable and appeared representative of the rime and mixed icing conditions for which they were calculated.

NOMENCLATURE

AOA	Angle-of-attack, degrees
C	Chord length, m

C_p	Pressure coefficient
d	Droplet diameter, μm
HTC	Heat transfer Coefficient, $W/m^2/K$
K_s	Roughness factor, m
LWC	Liquid Water Content, g/m^3
MVD	Median Volume Diameter, μm
P	Free stream pressure, Pa
s	Surface distance, cm
t	Ice accretion time, seconds
T	Free stream temperature, K
V	Free stream velocity, m/s
β	Collection efficiency

I. INTRODUCTION

The last 15 years has brought great changes in the computer software and hardware industry, changes which have given the design engineer a larger more sophisticated set of tools. A literal explosion of software has effected every level and aspect of engineering design. Engineers now have quick, and accurate tools at their fingertips to handle just about any design task imaginable. Tasks that were once unmanageable or manageable only by small Computational Fluid Dynamic (CFD) groups on expensive machines are now tractable by the ordinary design engineer. Computer programs that once took 10 hours of computer time and 2 days of turnaround time can now be done overnight on powerful, inexpensive workstations. Design tasks that were once empirically based "arts" are now analytically based sciences. One such area that has benefitted greatly from these changes has been the design of aircraft ice protection systems.

The task of aircraft ice protection system design which was previously one of subjectivity, based heavily on correlation and extrapolation, and carried out by highly experienced individuals is now one of objectivity, based on sound models and carried out by minimally experienced engineers. Historically systems have been designed using the methods of ADS-4 (ref. 1). This entailed interpolation or extrapolating from previously tested conditions and configurations. If a configuration or condition didn't exist in ADS-4 then various forms of extrapolation were used. As the aircraft industry progressed the newer designs were less and less similar to those in the ADS-4 database and the task of interpolation or extrapolation became harder and riskier. With the advent of the computer age numerical methods were made available, reducing the guess work. Many 2D and some 3D methods are now available to aid the user in designing an aircraft ice protection system (ref. 2-6). This paper outlines one such 3D method and presents validation for a variety of 3D geometries.

Flow, trajectory and ice accretion calculations were made and compared to experiment for several 3D geometries using the NPARC flow solver (ref. 7) and the grid based NASA Lewis 3D ice accretion code LEWICE3D (ref. 6). The cases were chosen to illustrate the flexibility and to provide validation for the computer code.

The grid based LEWICE3D code is very similar to the panel based version and incorporates the same trajectory and ice accretion methodology. The codes are different, in that the grid based code does not incorporate a flow solver but is dependent on the user to supply one. Several advantages of this are the ability to handle a users particular flow solver and the fact that the grid based trajectory codes are significantly faster than the panel based trajectory codes. The code can handle generic multi-block, structured or unstructured grids with symmetry planes. Performance differences can be as high 200 to 1 between the panel and grid based methods with a typical grid based case (single section of interest, single drop size) taking about 2.5 minutes on an SGI Model Power Challenge computer.

Computational and experimental results are presented for flow, and collection efficiency for 6 geometries. These cases included two spheres, a swept MS(1)-317 wing, a swept NACA-0012 wing tip, an axisymmetric inlet and a Boeing 737-300 inlet. All of the flow calculations were made using the NPARC flow solver except for the spheres. An analytical flow solution was used for the sphere cases. All of the aerodynamic and collection efficiency data were taken during the recent impingement efficiency tests, under a program funded by NASA and the FAA and carried out by Wichita State University, Boeing Military Airplanes and NASA (ref. 8), except for the spheres. The impingement efficiency data for the spheres was obtained during some of the early IRT impingement efficiency tests in the 1950's (ref. 9).

I. EXPERIMENT

B. EXPERIMENTAL APPARATUS

The aerodynamic and impingement efficiency tests were carried out in the NASA Lewis Icing Research Tunnel (IRT). The test equipment included the IRT (fig. 1), the ESCORT data system, a special spray system for the impingement tests (fig. 2), a laser reflectometer for impingement efficiency data reduction (fig. 3), and the six models (fig. 4-8).

The IRT facility can provide a range of airspeeds, angles-of-attack, temperatures, liquid water contents (LWC), and drop sizes (ref. 10). The IRT has a 2.47 m x 1.82 m test section with a maximum airspeed of 134 m/s (empty tunnel). Angle-of-attack is controlled by a movable turntable to which the models are mounted. A refrigeration system allows year-round testing at temperatures from -29° C to 10° C. The spray system located upstream of the test section can provide a cloud with a range of LWC of .25-3.0 gm/m^3 and a median volume drop (MVD) size range of 12-40 μm.

The Escort system was developed at Lewis to aid in storage, processing, and analysis of large amounts of data (e.g. temperature, pressure) produced in various experiments at Lewis Research Center. In this test Escort was used to store tunnel total temperature, total pressure, free stream airspeed, surface pressure, produce real time calculations and display pertinent parameters. The storage sequence for each data point was initiated by the researcher in the control room. A separate program was used to do a more complete post run analysis.

The spray requirements for the impingement tests precipitated the need for a different spray system (fig. 2) than was available in the IRT (ref. 8). The IRT spray system could not pro-

duce the short (2-5 seconds), stable sprays (i.e. constant LWC and drop size) required to prevent blotter strip saturation. There were also concerns that the dye would contaminate the IRT spray system. The new system consisted of 12 nozzles and a supply tank located at the IRT spray bar station (fig. 2). The system featured short supply lines which enabled short, stable sprays.

One unique feature of the current technique is the laser reflectometer used to determine the local collection efficiency (fig. 3). The device measures the local reflectance of the blotter strip and correlates this to the local collection efficiency. The device saved considerable time in the data reduction of the blotter strips.

The sphere data used here was obtained during impingement tests in 1957 (ref. 9). Figure 4 shows a schematic of the IRT sphere test configuration. Two spheres having diameters of 15.04 cm and 45.72 cm were tested at several MVD's. Both models were made of laminated mahogany.

The swept MS(1)-317 model was constructed for the IRT test section (fig. 5). The model was full span (6 foot) and had a three foot chord. The model had a 30° sweep angle and was made of mahogany. The model was unusual in that the MS(1)-317 coordinates were applied in the free stream flow direction and that the trailing edge was closed. This unusual design was thicker than the usual swept MS(1)-317 defined in the leading edge normal direction.

The swept NACA-0012 wing tip model (fig. 6) was designed to have variable sweep and so that it could be tested in both the IRT and on Twin Otter Icing Research Plane. The model had was made of mahogany and had several removable end sections which allowed sweep angle configurations of 0, 15, 30 and 45 degrees. The model had a chord of .4399 m (leading edge normal direction) and a leading edge length of .7111 m.

The axisymmetric inlet and 737-300 inlet models (figs. 7,8) were both .2547 scale. The models were provided by Boeing Commercial Airplane Company. The axisymmetric inlet was outfitted with 34 static pressure taps while the 737-300 had 88. The axisymmetric inlet did not have a centerbody, although the model was tested with a centerbody mount. The 737-300 had a conical centerbody.

B. EXPERIMENTAL TESTING

Two types of testing were done in the IRT: aeroperformance and impingement efficiency testing. The aero-performance testing involved taking surface pressure measurements. The impingement efficiency testing involved the use of a dye tracer technique to measure the location and amount of water impinging on the model.

Surface pressures were measured on the inlet models using the ESCORT system. Pressure measurements were taken at an airspeed of 77 m/s, at angles-of-attack of 0° and 15° and inlet mass flows of 7.8 kg/s and 10.4 kg/s with the spray system off. Three sets of pressure measurements were taken for each configuration to establish repeatability of the data.

The experimental technique used in the current tests to determine the impingement char-

acteristics of a body is one that was developed on the early 1950's with a few modifications (ref. 8). The technique involved spraying a dye-water solution of a known concentration onto a model covered with blotter strips. Figure 9 shows a typical blotter installation for the 737-300 inlet. The result was that the local impingement efficiency rate was reflected on the blotter strips as a variation in color intensity. That is, the areas of higher impingement rate are darker and those with lower impingement rate are lighter.

Several steps were necessary to prepare the IRT for impingement testing. The specially designed spray system had to be installed and adjusted to produce a uniform cloud. The local LWC had to be measured at each blotter strip location (with the tunnel empty) for every spray and tunnel condition to account for any cloud nonuniformity that existed after the final spray adjustment. After these adjustments and measurements were made the model was inserted and tested. Each points was repeated five times to obtain a statistical average.

A typical test point for an airfoil involved several steps. The model was cleaned and blotter strips were attached at points of interest. Figure 9 shows a typical blotter strip installation for the 737-300 inlet and illustrates the angular reference system used in presenting the data.The spray was then made, the blotter strips were removed, and labeled, and the model was cleaned and made ready for the next condition.

Table I summarizes the test matrix for the impingement tests. All of the models were tested for two drop sizes and at two angles-of-attack except for the spheres. The 45.72 cm sphere was tested for MVD's of 11.5, 14.7, 16.7 and 18.6 μm the 15.04 cm sphere was tested for MVD's of 11.5, 16.7 and 18.6 μm.

II. ANALYTICAL METHOD

The NPARC flow solver was used to generate all of the grid based flow solutions except for the spheres and the NASA Lewis grid based ice accretion code (LEWICE3D) was used for the trajectory and ice accretion analysis. An analytical flow solution was used for the grid based sphere cases. The LEWICE3D panel based computer program has been used in previous calculations of isolated, finite wings and full aircraft (ref. 11-15). The work presented here represents the first application of the computationally similar grid based LEWICE3D to various bodies.

NPARC, formerly PARC, is a 3D CFD flow solver for application to compressible internal and external flows (ref. 7). The code implements the Beam-Warming implicit algorithm to solve the steady-state Euler or Navier-Stokes equations, as did the ARC3D code from which NPARC was derived. An optional pseudo-Runge-Kutta algorithm allows NPARC to compute unsteady flows. A Jameson-style artificial viscosity model is included to stabilize the solution. The viscous mode of NPARC allows prediction of turbulent flow via the availability of several turbulence models including P.D. Thomas, Baldwin-Lomax, Chien k-epsilon, Baldwin-Barth, and RNG. NPARC accepts multi-block structured grids as long as adjacent grids overlap by at least one grid cell at their interfaces. Blocks may overlap by wide margins, or be embedded entirely within other blocks, to ease the modeling of difficult geometries as well as to resolve local geometry and flow features. Additional modeling flexibility is provided by NPARC's ability to allow internal walls,

whereby portions of a grid block are cordoned off from the solution by application of boundary conditions to walls internal to a grid block.

For the current study, NPARC was run steady-state and inviscid (Euler mode). The two inlet geometries and the NACA 0012 wing with tip were each modeled using two-block grids while the MS-317 required only one block. Numerous boundary conditions are available to the NPARC user. Examples employed in the current study include freestream, slip-walls, specified mass-fluxes, imposed static pressures, collapsed-point pole singularities, block interfaces, and a C-grid wake-cut for lifting surfaces.

NPARC calculation times varied for the different geometries depending upon the number of grid points, the number of blocks and the type of boundary conditions used. The Euler flow calculations were made using version 2.0 of NPARC on one processor (R8000) of an SGI Power Challenge computer. The calculations were considered converged when the L2 residuals (ref. 7) dropped 5 orders of magnitude. One iteration took about .87 cpu-seconds per 10,000 grid points, regardless of geometry. For the wing geometries convergence took about 5000 iterations which yielded calculation times of 5 hours and 25 hours respectively for the swept MS(1)-317 wing and the swept NACA-0012 wing tip respectively. The calculation time for swept NACA-0012 wing was about 5 times larger than that of the swept MS(1)-317 because the grid used to model the swept NACA-0012 wing tip contained about 5 times the number of points used for the swept MS(1)-317 wing. For the two inlet geometries, convergence occurred after about 15000 iterations which resulted in calculation times of 130 hours and 80 hours for the axisymmetric and Boeing 737-300 inlets respectively. The inlets required larger numbers of iterations because of the way in which the mass flow boundary condition is applied. NPARC iterates on the inlet exit pressure until the correct mass flow is calculated through the inlet exit.

The LEWICE3D grid based code incorporates trajectory, heat transfer and ice shape calculation into a single computer program with a multitude of capabilities. The code can handle generic multiblock structured grid based flow solutions, unstructured grid based flow solutions and simple cartesian grids with surface patches (allows generic panel code users a computationally efficient mode for ice shape determination). The code can handle overlapping and internal grids and can handle multiple planes of symmetry. Calculations of arbitrary streamlines and trajectories are possible. The code has the capability to calculate tangent trajectories and impingement efficiencies for single droplets or droplet distributions. Ice accretions can be calculated at arbitrary regions of interest in either a surface normal or tangent trajectory direction.

The methodology used in the LEWICE3D (ref. 6) analysis can be broken into six basic steps for each section of interest at each time step. In the first step the flow field is generated by the user. Secondly, surface streamlines are calculated. Thirdly, tangent trajectories are calculated at the region of interest. An array of particles is released between the tangent trajectories in the fourth step. These impacting particles are used to calculate collection efficiency as a function of surface position. The fifth step involves interpolating or extrapolating the collection efficiencies onto the streamlines. In the sixth step the ice accretion for the streamline is calculated.

There are three basic program elements contained in the LEWICE3D jobstream; a trajectory analysis, a streamline analysis and an ice accretion analysis. The trajectory analysis is basi-

cally that of Hillyer Norment (ref. 16) with modifications by Bidwell (ref. 6). At the heart of the trajectory analysis is the variable step predictor-corrector integration scheme by Krogh (ref. 17). The surface streamline analysis uses a variable step size fourth-order Runge-Kutta integration scheme developed by Bidwell (ref. 6). The ice accretion model is basically that of the LEWICE2D code applied along surface streamlines (ref. 3).

LEWICE3D calculation times varied for the different cases depending upon the drop size, the number of trajectories, the number of grid points, number of grid blocks, and type of grid blocks. The LEWICE3D calculation times are heavily dependent upon grid size and structure because the largest portion of the LEWICE3D calculation time (greater than 99%) is spent calculating velocities at specified points, which involves searching through the grid block for the cell in which the point is located. The search algorithm employed is dependent upon integration step size, grid cell size and orientation, the number of grid cells, the number of grid blocks and the orientation of the grid blocks. The trajectory integration time for the cases varied from .2-10. seconds. Average trajectory integration time was approximately 1.25 seconds for all of the cases. Approximately 100 trajectories were required for each drop size at each section-of-interest. This resulted in calculation times of approximately 1000 seconds for the wings and spheres (one section-of-interest, 7 bin distribution) and approximately 5000 seconds for the inlet cases (5 sections-of-interest, 7 bin distribution).

III. ANALYSIS

Surface velocity, heat transfer, collection efficiency, and ice shapes results are presented for the five geometries tested. Ice shape calculations were made for two icing conditions simulating a rime and a mixed condition. Comparisons to experimental collection efficiency are made for all of the cases and to experimental surface mach number or coefficient of pressure where available. Discussions of the icing conditions chosen, the LEWICE3D program parameters used, and of the individual analysis are given below.

Two icing conditions were calculated for each data point in the collection efficiency matrix (table I) for each model except for the sphere. Icing calculations were only run for the smallest and largest MVD droplets for the spheres. The icing conditions were chosen to loosely match a rime and a mixed hold condition. For the rime condition an icing time of 30 minutes, an LWC of .2 g/m^3 and a temperature of 243.1 K were used. For the mixed condition an icing time of 30 minutes, an LWC of .695 g/m3 and a temperature of 263.7 K were used.

The grid based LEWICE3D computer program parameters were chosen from experience, correlations and a desire to limit the computational resources required. A 7 bin droplet distribution was used in the calculations (table II). For the spheres cases a Langmuir-D distribution (ref. 18) was used. This distribution was chosen as representative of the multicylinder and Jakowski airfoil data taken by early researchers (ref. 9). For the remaining cases experimentally measured droplet distributions (ref. 8) were used for the calculations (table II). These distributions were measured using laser droplet sizing instruments. The icing calculations were made using a single ice accretion time step. A LEWICE roughness parameter (ref. 3) of .5mm was used for all of the cases.

Figures 10-14 depict the results for the two sphere calculations. A single block C-grid was

used for the calculations (fig. 4b). The grid, which used a y-plane of symmetry contained 92 radial points, 91 chordwise grid points and 90 spanwise points. An incompressible, inviscid analytical flow solution was used to generate the velocities at the grid points. Figure 12a shows the comparison between the analytical and experimental coefficient of pressure for the front of the sphere. The agreement is excellent. The stagnation heat transfer also compares well to previous data. The collection efficiencies compare well for both spheres in both limits of impingement and maximum collection efficiency except for the 45.15 cm sphere at 18.5 μm. For this case the limits of impingement are slightly underpredicted and the maximum collection efficiency is severely underpredicted. This discrepancy could be due to relative error in the experiment or possibly due to a measurement error of MVD or of droplet distribution in the early experiments. The average repeatability for the impingement data is about +- 10%. Maximum differences can be as high 40% for some cases.These large differences generally occur in very small regions near the peak collection efficiency for geometries with relatively sharp leading edges. These differences are not considered as a serious condemnation of the experimental technique because they occur for over small regions and do not involve much total water. Modern calibrations of the IRT nozzles, which are similar to those in the 1950's, differ considerably from the early calibrations in both MVD and distribution at the 18.5 μm condition. Future work is planned to explore this discrepancy. Figure 14 depicts the analytically predicted ice shapes for the spheres. Although no experimental data was available for comparison the ice shapes look indicative of the rime and glaze conditions from which they were generated.

The swept MS(1)-317 results are shown in figures 15-18. A single-block C-grid was used for the calculations (fig. 5b). The grid contained 5 spanwise grid planes, 277 chordwise grid points and 30 radial grid points. At the first and last spanwise grid planes, a contiguous boundary condition was imposed which communicated flow information directly between the first and last plane, effectively making the calculation model a wing of infinite span. No attempt was made to represent the tunnel walls in the grid. The figures depict parameter plots of percent chord or surface distance along a cut in the flow direction at the center span location. Surface distance was measured from the highlight, with positive values being on the underside of the wing and negative values being on the upper side of the wing. The ice shapes were generated in a leading edge normal direction.

Figures 15, 16 show the coefficient of pressure and heat transfer distributions for the 0 and 8 degree conditions. Although no experimental data was available for these conditions the distributions look reasonable.

The collection efficiency comparisons for the swept MS(1)-317 are shown in figure 17. In general, the impingement limits are overpredicted and the maximum collection efficiency is underpredicted. The comparisons appear reasonable considering the experimental repeatability for all but the 20 μm, 8° AOA case for which the maximum collection efficiency is severely underpredicted. The discrepancy is probably due to the less than idealistic flow realized for the 8° AOA case and the inability of the steady Euler calculation to pick it up. Flow separation may have occurred for this case due to the unusually thick (i.e. 17% in the flow direction) nature of the model, the relatively high AOA, and finite span of the tunnel.

Figure 18 shows the ice shapes for the rime and mixed conditions. Although no experi-

mental data were available for these conditions the ice shapes looked reasonable and representative of the conditions for which they were generated. The rime shapes reflect the heavy influence of the collection efficiency distribution and the mixed shapes reflect the heavy influence of the heat transfer distribution. For the rime case the droplets will essentially freeze upon impact giving rise to a ice thickness distribution and ice shape that resembles the collection efficiency distribution. For mixed and glaze shapes more water is available at the leading edge than can immediately freeze resulting in a freezing fractions of less than one. This implies that the ice thickness distribution, and hence the ice shape, will resemble the heat transfer coefficient distribution. If transition occurs horns will be formed near the transition location due to the sharp increase in heat transfer at transition.

The results for the swept NACA-0012 wing tip are shown in figures 19-22. A 2 block grid was used for the calculations (fig. 6b). A C-grid with 25 spanwise stations, 183 chordwise stations and 35 radial stations was used to cover the wing the from the root to tip. A second C-O grid which had 92 chordwise points, 35 radial points and 15 circumferential grid points was used to model the circular endcap. No attempt was made to include the IRT tunnel walls or the model support structure in the grid construction. The grid contained a plane-of-symmetry at the wing root. The parameter plots involving surface distance and chord length were made along vertical cuts in the flow direction. Surface distance was measured from the highlight, with positive values being on the underside of the wing and negative values being on the upper side of the wing. The ice shapes were generated in a leading edge normal direction.

Figures 19 and 20 show the coefficient of pressure distributions and heat transfer distributions. The results look reasonable. Although no pressure or heat transfer data was available comparisons to unswept data using the infinite swept assumption (i.e. multiplying the unswept coefficient of pressure by the square of the cosine of the sweep angle and the heat transfer coefficient by the square root of the cosine of the sweep angle) were good. When LEWICE2D results were corrected for sweep, the maximum pressure coefficient for the 0° AOA case was -.317. This agreed well with the -.304 value calculated using LEWICE3D. When the LEWICE2D stagnation heat transfer coefficient was corrected for sweep a value of 374 $W/m^2/K$ was found for the 0° AOA case. This agreed reasonably with the LEWICE3D value of 340 $W/m^2/K$ considering the differences in the coefficient of pressure at this angle-of-attack.

The collection efficiency results for the swept NACA-0012 swept wing tip are shown in figure 21. The agreement in overall shape of the curve, area under the curve and maximum collection efficiency look good considering the repeatability of the data. The worst agreement occurs for the 8° AOA, 20 μm MVD case where the maximum collection efficiency is underpredicted by 36% and the lower impingement limit is overpredicted by a whopping 200%. The disagreement in the lower impingement at the higher angle-of-attack, which is not uncommon for 2D and 3D cases, is disconcerting. But it must be pointed out that these type of absolute comparisons are not quite fair in judging the validity of the theoretical method. The experimental technique used here does not yield exact impingement limits. The subtraction technique used in the data reduction combined with the insensitivity of the laser to low collection efficiencies, which occur near the impingement limits, gives rise to an error in the estimation of the impingement limit. Further, it is difficult to know exactly how large this error is because no other independent, more accurate method is available for providing imipingiment limit measurement. Keeping this in mind compar-

ing the collection efficiency curves in the 8° AOA, 20 μm MVD case (fig. 21d) we might consider the agreement for the lower impingement limit reasonable. The agreement in the collection efficiency from the 3-10 cm region is excellent, after which the experimental data ends rather abruptly and the analytical results tend to zero in a smooth fashion.

Ice shapes for the swept NACA-0012 wing tip are shown in figure 22. The ice shapes were reasonable considering the conditions for which they were generated, the collection efficiency distribution and the heat transfer distribution.

Figures 23-30 summarize the results for the axisymmetric inlet. A 2 block grid with a y-plane of symmetry was used for calculations (fig. 7b). The first block consisted of an O-grid which extended from the rear of the inlet to freestream. The grid contained 29 axial grid points, 29 radial grid points and 45 circumferential grid points. Embedded inside the first block, the second block consisted of a C-O grid which modeled the inlet geometry. The grid block had 99 chordwise grid points, 35 radial grid points and 89 circumferential grid points. The amount of mass-flow through the inlet, known from the experiment, was imposed on the exit plane of the inlet grid by use of NPARC's mass-flow boundary condition. The ice shape and parameter plots were all made along radial cuts parallel to the flow direction.

The surface mach number and heat transfer distributions are presented in figures 23,24. In general, the agreement between the experimental and computed surface mach number is excellent. Although no experimental data was available for the heat transfer distributions, the analytical results appear reasonable in that they follow trends set by the surface mach number distributions (i.e where there are high mach number gradients there are high heat transfer coefficients). The heat transfer distribution trends with respect to mass flow and angle-of-attack also look reasonable. In general, increasing mass flow caused the peak heat transfer to increase on the inside of the inlet and to decrease on the outside of the inlet. Increasing the angle-of-attack resulted in opposite trends for the heat transfer on the lower and upper inlet lips. For the lower inlet lip the peak heat transfer decreased on the inside of the inlet and increased on the outside of the inlet. For the upper lip the peak heat transfer increased on the inside of the inlet and decreased on the outside of the inlet.

Figures 25, 26 show the collection efficiency results for the axisymmetric inlet. The agreement is excellent. The experimental and computational results agree well in shape of curve, area under the curve, maximum collection efficiency and impingements limits.

The computed ice shapes are presented in figures 27-30. Although no experimental data was available the results looked consistent with the conditions for which the shapes were generated, and with the collection efficiency distribution and with the heat transfer distribution. The location, size and shape of the ice shapes can be more easily understood if we think of the results in terms of local angle-of-attack. If we think in terms of local angle-of-attack of the inlet lip then 2D wing icing experience can be used. We will define the local angle-of-attack to be measured in the radial plane containing the inlet lip, and measured from the highlight of the lip with values towards the inside of the inlet being negative and those towards the outside of the inlet being positive. In this system for a axisymmetric inlet at 0 AOA the local angle-of-attack will be the same at any radial cut. The local angle-of-attack is a function of inlet mass flow and inlet angle-of-

attack. At a given inlet angle-of-attack the local relative angle-of-attack increases with decreasing mass flow. At a given mass flow increasing the angle-of-attack increases the relative angle-of-attack of the lower inlet lip, and decreases the relative angle-of-attack of the upper inlet lip. From 2D experience we know that as we increase angle-of-attack the ice shapes will accrete more towards the underside of the geometry. From this and our above definition of local angle-of-attack we can make several generalizations about the location of the ice shapes. At a given positive inlet angle-of-attack the ice shape will transition from more towards the outside of the inlet to more towards the inside of the inlet as we traverse from the lower lip around the inlet to the upper lip. For a given inlet angle-of-attack increasing the mass flow will result in an ice shape that is more towards the outside of the inlet. These trends are more readily observable for the mixed ice conditions in the figures.

The results for the 737-300 inlet are shown in figures 31-38. A 2 block grid with a y-plane of symmetry was used for calculations (fig. 8b). The 2-block computational grid was arranged in the manner of the previously described axisymmetric grid. The first grid block contained 42 axial grid points, 42 radial grid points and 25 circumferential grid points. The second grid block had 80 chordwise grid points, 30 radial grid points and 73 circumferential grid points. As for the axisymmetric inlet, mass flow quantities measured in the experiment were imposed on the exit plane of the Boeing 737-300 inlet.The ice shape and parameter plots were made along radial cuts parallel to the flow direction.

The surface mach number and heat transfer distributions are presented in figures 31,32. In general, the agreement between the experimental and computed surface mach number is good. Although no experimental data was available for the heat transfer distributions, the analytical results appear reasonable in that they follow trends set by the surface mach number distributions.

Figures 33, 34 show the collection efficiency results for the 737-300 inlet. The agreement is excellent. The experimental and computational results agree well in shape of curve, area under the curve, maximum collection efficiency and impingements limits.

The computed ice shapes are presented in figures 35-38. Although no experimental data was available the results looked consistent with the conditions for which the shapes were generated, and with the collection efficiency distribution and with the heat transfer distribution.

V. CONCLUSION

The grid based LEWICE3D-NPARC combination proved to be an inexpensive, flexible, accurate ice protection system design tool. The flow and ice accretion calculations were done quickly, cheaply and accurately for a range of 3D configurations.

The NPARC, grid based LEWICE3D, SGI Power Challenge computer combination was, in general, inexpensive to operate. The Euler flow calculations took on the average of 15 hours for an isolated wing case and 100 hours for an isolated inlet case on the SGI Power Challenge computer. The ice accretion calculations required about 20 minutes per section-of-interest using a

seven bin distribution. These run times imply LEWICE3D execution times on the order of several hours for full aircraft configurations.

The NPARC and grid based LEWICE3D codes proved to be flexible. The codes were used to calculate ice accretions for cases with external and internal flow with and without planes of symmetry. The codes were used with multiblock grids with overlapped and imbedded blocks and with a variety of boundary conditions.

In general, the calculations for surface velocity, heat transfer, collection efficiency and ice shape compared well with experiment where data was available and with intuition where no data was available. The surface velocities for spheres and inlets agreed well with experiment. Although no experimental data was available for the swept wings the surface pressure compared reasonably to unswept results using the infinite sweep correction. The stagnation heat transfer for the sphere compared well with experiment. The stagnation heat transfer for the swept NACA-0012 wing tip compared reasonably well to 2D results using the infinite sweep correction. Although no heat transfer data was available for the inlets, the results correctly followed velocity gradient, mass flow and angle-of-attack trends and appeared reasonable. The calculated collection efficiency compared favorably for all cases considering the inviscid flow approximation used and the repeatability and accuracy of the collection efficiency data. The ice shape predictions appeared reasonable and representative of the conditions from which they were derived. The rime and mixed shapes followed trends set by the collection efficiency and heat transfer coefficient, respectively.

REFERENCES

1. Bowden, D.T., Gensemer, A.E.,and Skeen, C.A., "Engineering Summary of Airframe Icing Technical Data," FAA ADS-4, December 1963.

2. Lozowski, E.P., and Oleskiw, M.M., "Computer Modeling of Time-Dependent Rime Icing in the Atmosphere," CRREL 83-2, Jan. 1983

3. Ruff, G.A., Berkowitz, B.M.," Users manual for the NASA Lewis Ice Accretion Prediction code (LEWICE)," NASA CR 185129, May 1990.

4. Cebeci, T., Chen, H.H., and Alemdaroglu, N., "Fortified LEWICE with Viscous Effects." AIAA Paper 90-0754, Jan. 1990

5. Cansdale, J.T., and Gent, R.W., "Ice Accretion on Aerofoils in Two-Dimensional Compressible Flow - A Theoretical Model," RAE TR 82128, January 1983.

6. Bidwell, C.S., and Potapczuk, M.G., "Users Manual for the NASA Lewis Three-Dimensional Ice Accretion Code (LEWICE3D)," NASA TM 105974, December 1993.

7. Cooper, G.K., and Sirbaugh, J.R., "PARC Code: Theory and Usage," AEDC-TR-89-15,

December 1989.

8. Papadakis, M., Elangonan, G.A., Fruend, G.A.,Jr., Breer, M., Whitmer, L., "An experimental Method for Measuring Water Droplet Impingement Efficiency on Two-and Three-Dimensional Bodies," NASA CR 4257, DOT/FAA/CT-87/22.

9. Lewis, J.P., Ruggeri, R.S. " Experimental Droplet Impingement on Four Bodies of Revolution," NACA TN 4092, December 1957.

10. Soedher, R.H., Andracchio, C.R., "NASA Lewis Icing Researcc Center Tunnel User Manual," NASA TM 82790, 1990.

11. Potapczuk, M.G. and Bidwell, C.S., "Swept Wing Ice Accretion Modeling," NASA TM 103114, January. 1990.

12. Potapczuk, M.G. and Bidwell, C.S., "Numerical Simulation of Ice Growth on a MS-371 Swept Wing Geometry," NASA TM 103705, January 1991.

13. Reehorst, A. L., "Prediction of Ice Accretion on a Swept NACA 0012 Airfoil and Comparisons to Flight Test Results," NASA TM 105368, January 1992.

14. Mohler, S.R., Bidwell, C.S., "Comparison of Two-Dimensional and Three-Dimensional Droplet Trajectory Calculations in the Vicinity of Finite Wings," NASA TM 105617, January 1992.

15. Bidwell, C.S.., "Ice Accretion Prediction for a Typical Commercial Transport Aircraft," NASA TM 105976, January 1993.

16. Norment, H.G., "Calculation of Water Drop Trajectories To and About Three-Dimensional Lifting and Non-lifting Bodies In Potential Airflow," NASA CR 3935, Oct. 1985.

17. Krogh, F.T. ,"Variable Order Integrators for Numerical solutions of Ordinary Differential Equations," Jet Propulsion Lab Technology Utilization Document No. CP-32308, Nov. 1970.

18. Langmuir, I., Blodgett, K.B. ,"A Mathematical Investigation of Water Droplet Trajectories", Army Air Forces Technical Report 5418, Feb., 1946.

TABLE I. - IMPINGEMENT EFFICIENCY TEST MATRIX.

Model Description*	AOA (Degrees)	Engine Suction Flow (kg/s)	MVD (μm)
15.04 cm Sphere**	-	-	11.5, 16.7, 18.6
45.72 cm Sphere**	-	-	11.5, 14.7, 16.7, 18.6
Swept MS(1)-317 Wing ‡	0, 8	-	16.4, 20.4
Swept NACA-0012 Wing Tip ‡	0, 8	-	16.4, 20.4
Axisymmetric Engine Inlet †	0, 15	7.8, 10.4	16.4, 20.4
Boeing 737-300 Engine Inlet †, ‡	0, 15	7.8, 10.4	16.4, 20.4

* All tests were performed at a tunnel air temperature of approximately 10° C, and at an indicated airspeed of approximatley 73-78 m/s.
** Models tested in 1957.
† Models tested in September 1985
‡ Models tested in April 1989

TABLE II. - DISCRETIZED DROPLET DISTRIBUTIONS USED IN CALCULATIONS.

% LWC	d(I)/MVD					
	MVD, 11.5 μm*	MVD, 14.7 μm*	MVD, 16.4 μm†	MVD, 16.7 μm*	MVD, 18.6 μm*	MVD, 20.4 μm†
5	.31	.31	.3161	.31	.31	.2770
10	.52	.52	.4981	.52	.52	.4460
20	.71	.71	.6872	.71	.71	.6617
30	1.00	1.00	1.000	1.00	1.00	1.0000
20	1.37	1.37	1.3737	1.37	1.37	1.5865
10	1.74	1.74	1.9614	1.74	1.74	2.2943
5	2.22	2.22	2.8288	2.22	2.22	3.2542

* Langmuir-D distribution.
† Distribution measured at AEDC.

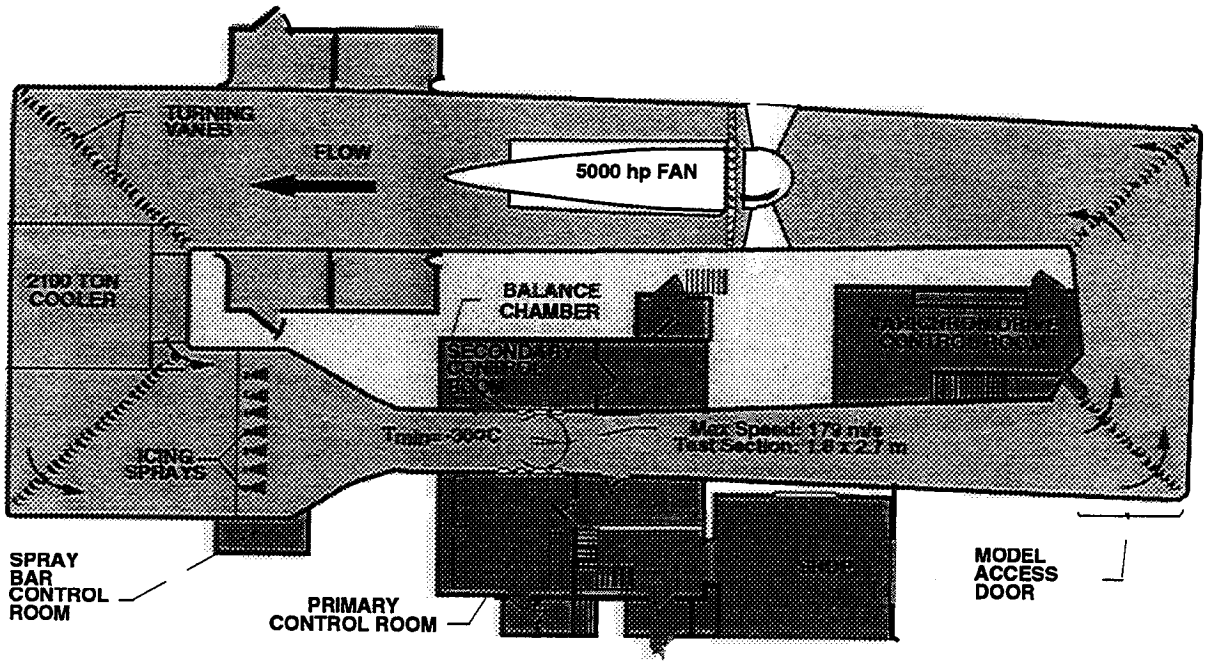

Figure 1. - NASA Lewis Icing Research Tunnel. Plan view.

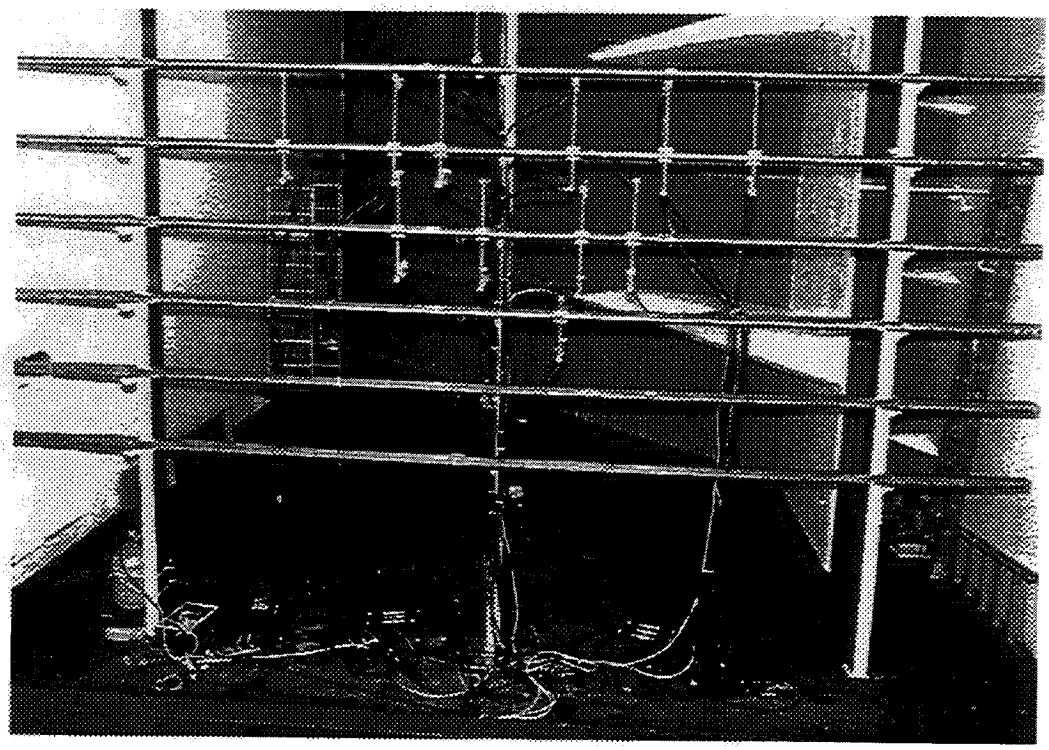

Figure 2. - Installation of spray sytem used for Icing Research Tunnel impingement tests.

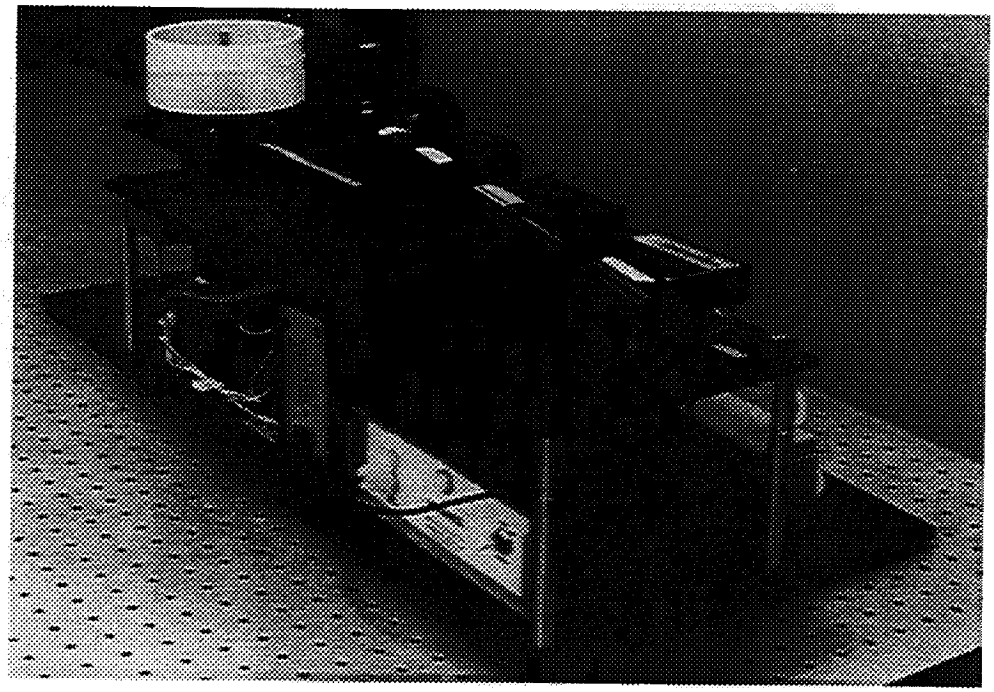

Figure 3. - Automated Reflectometer used to reduce impingement data.

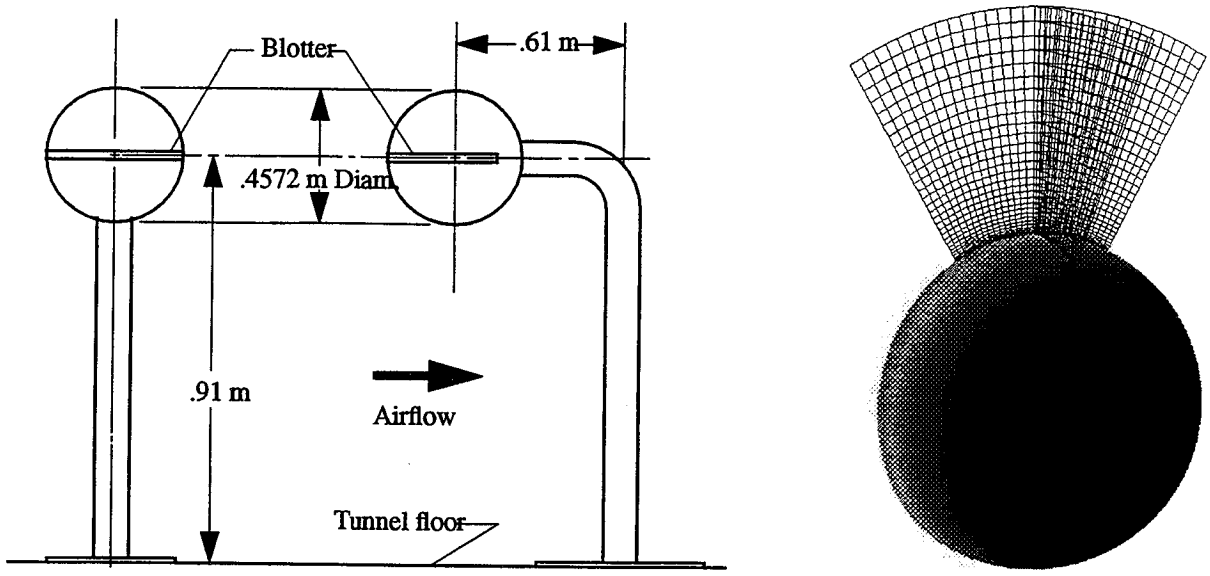

(a) Sketch of sphere installation in IRT.

(b) Grid model.

Figure 4. - Sphere model.

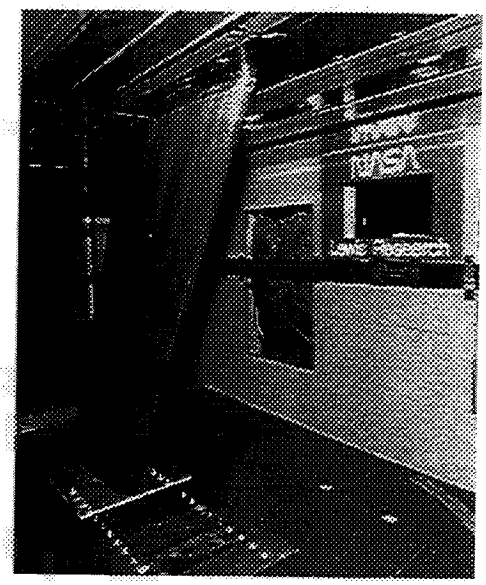

(a) Installation in IRT.

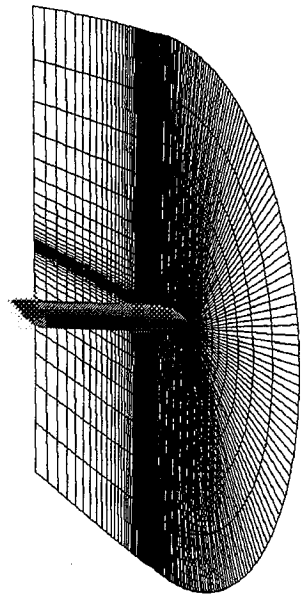

(b) NPARC grid model.

Figure 5. - Swept MS(1)-317 wing.

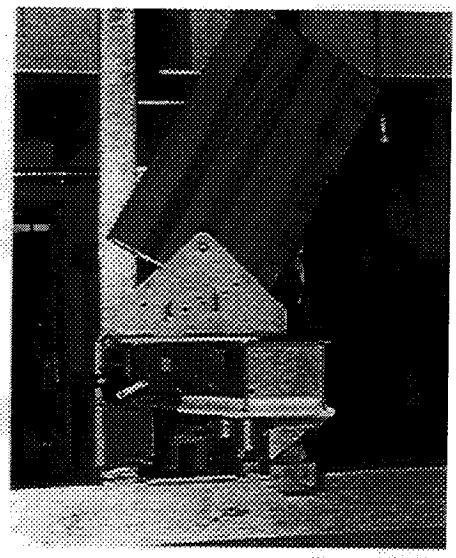

(a) IRT Test model.

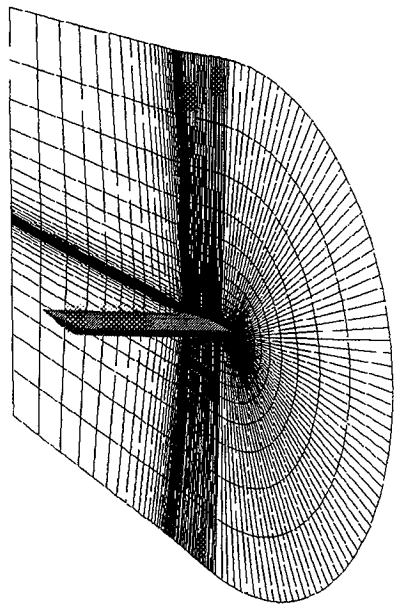

(b) NPARC grid model.

Figure 6. - Swept NACA-0012 wing tip.

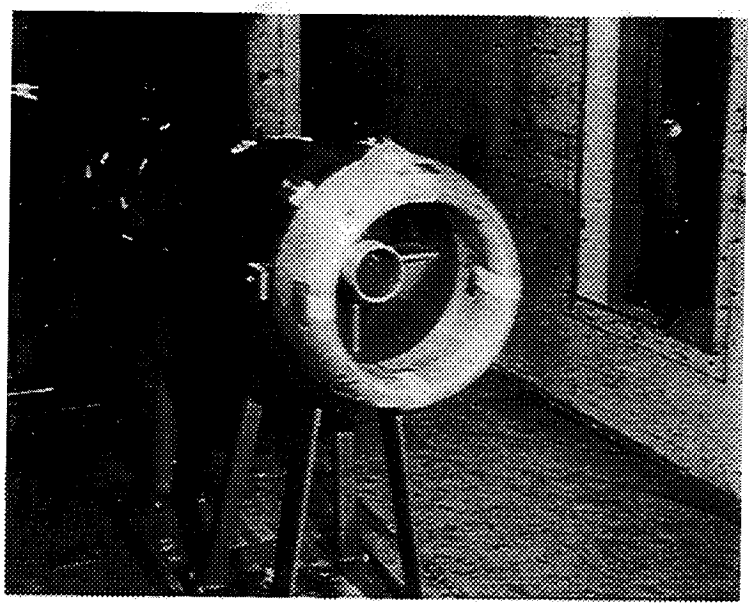

(a) Installation in IRT.

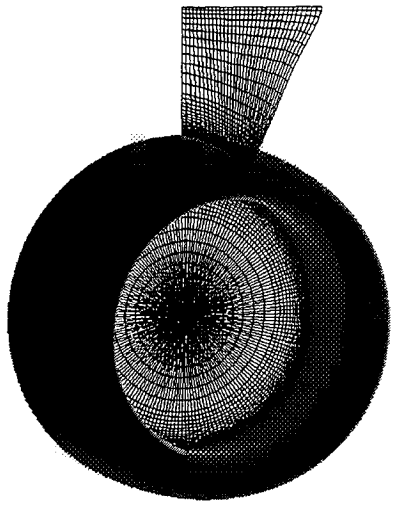

(b) NPARC grid model.

Figure 7. - Axisymmetric inlet.

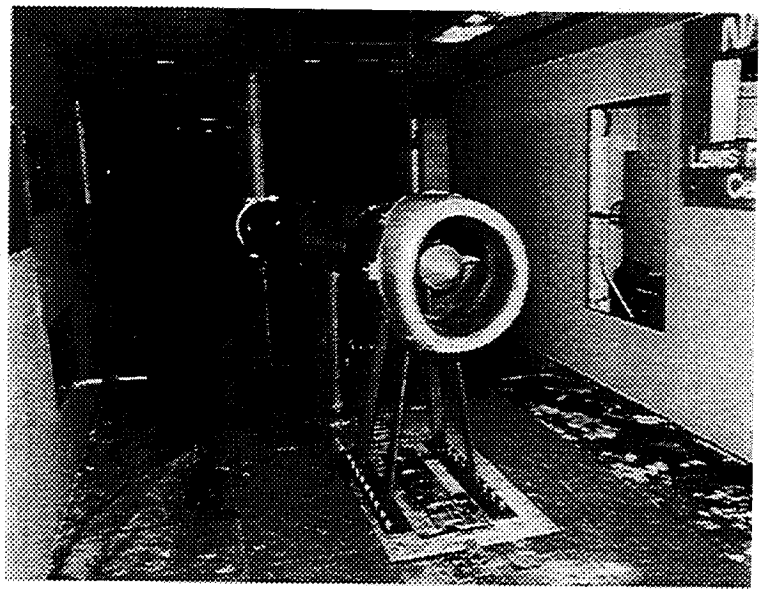

(a) Installation in IRT.

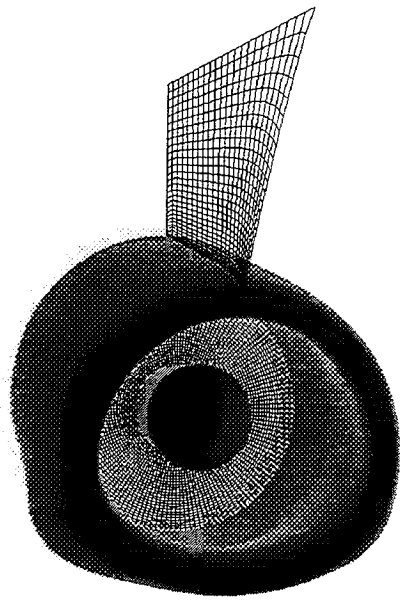

(b) NPARC grid model.

Figure 8. - Boeing 737-300 inlet.

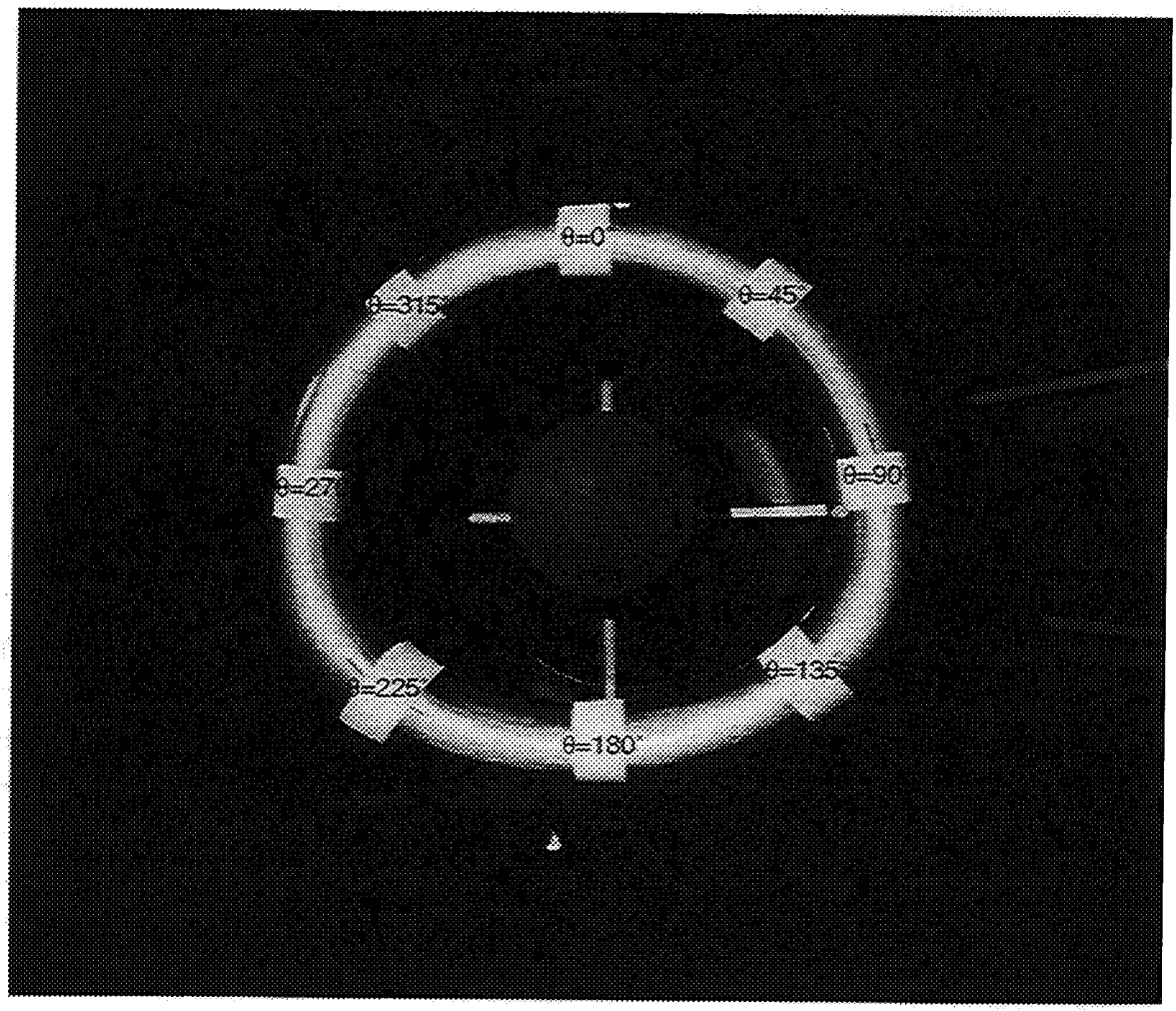

Figure 9. - Illustration of inlet blotter strip orientation..

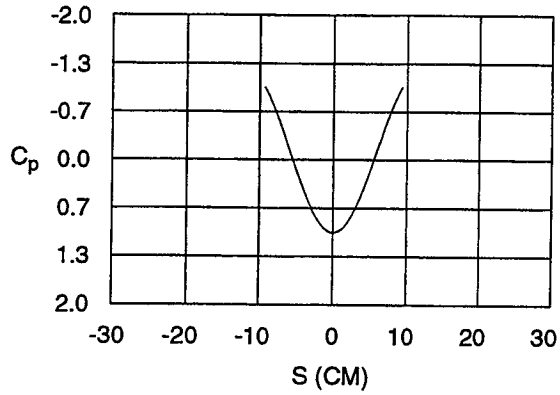

(a) Coefficient of pressure.

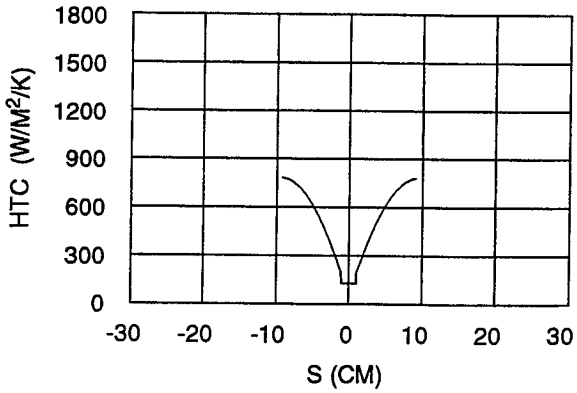

(b) Heat transfer coefficient

Figure 10. - Theoretical coefficient of pressure and heat transfer coefficient for a 15.04 cm sphere. Airspeed, 75 m/s; static temperature, 7° C; static pressure 95840 Pa.

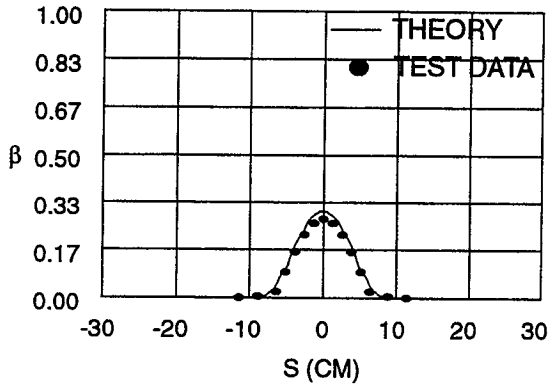

(a) MVD, 11.5 μm.

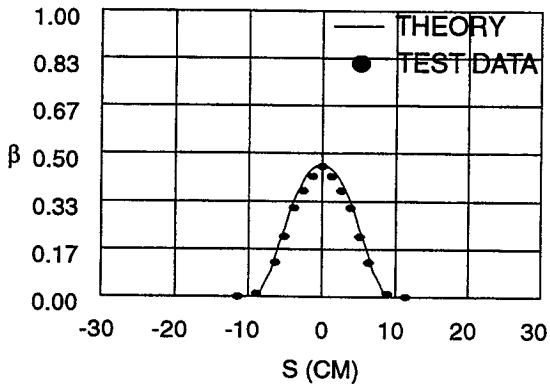

(b) MVD, 16.7 μm.

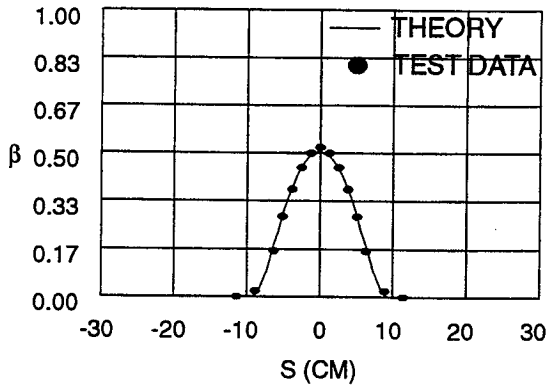

(c) MVD, 18.6 μm.

Figure 11. - Comparison of experimental and theoretical collection efficiency for a 15.04 cm sphere. Airspeed, 75 m/s; static temperature, 7° C; static pressure 95840 Pa.

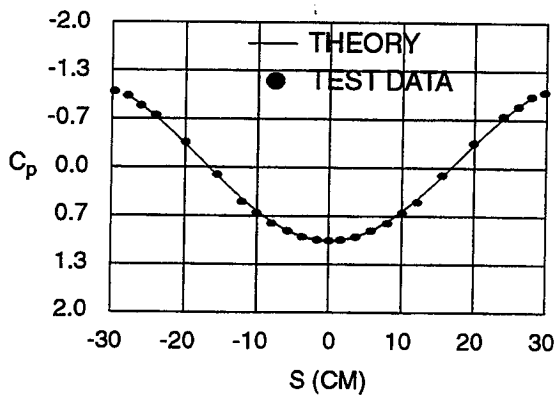

(a) Coefficient of pressure.

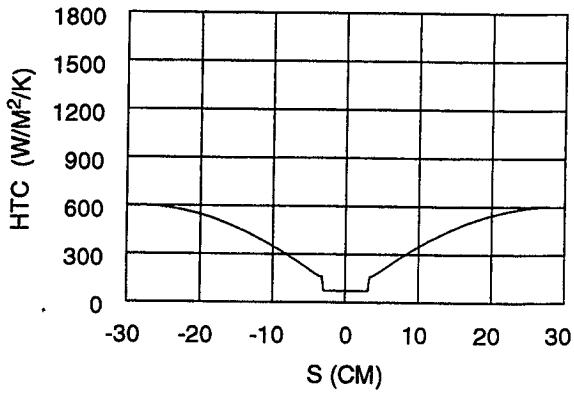

(b) Heat transfer coefficient

Figure 12. - Theoretical coefficient of pressure and heat transfer coefficient for a 45.72 cm sphere. Airspeed, 75 m/s; static temperature, 7° C; static pressure 95840 Pa.

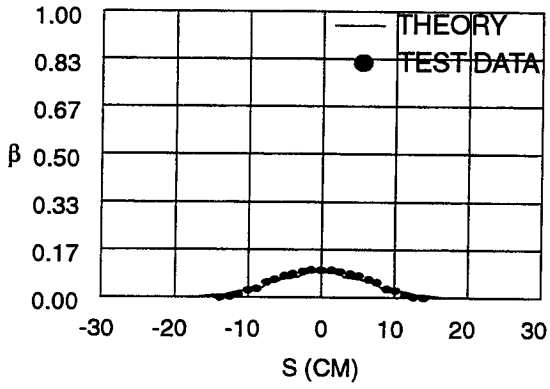

(a) Median volume diameter, 11.5 μm.

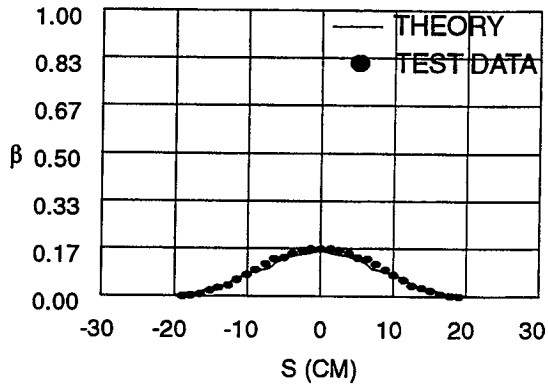

(b) Median volume diameter, 14.7 μm.

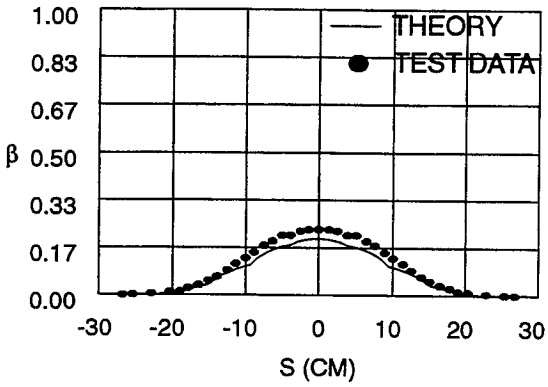

(c) Median volume diameter, 16.7 μm.

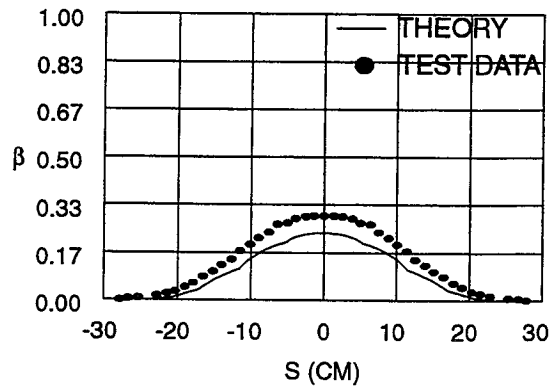

(d) Median volume diameter, 18.6 μm.

Figure 13. - Comparison of experimental and theoretical collection efficiency for 45.72 cm sphere. Airspeed, 75 m/s; static temperature, 7° C; static pressure 95840 Pa.

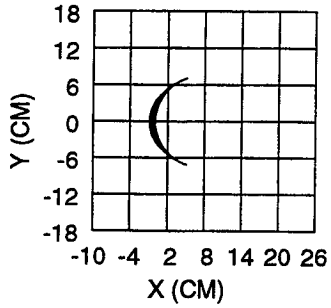

(i) Sphere Diameter, 15.04 cm; MVD, 11.5 μm.

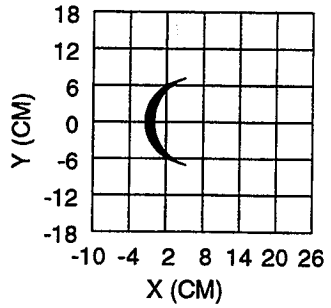

(ii) Sphere Diameter, 15.04 cm; MVD, 18.6 μm.

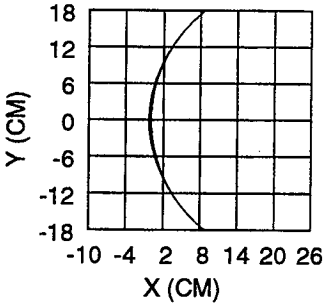

(iii) Sphere Diameter, 45.72 cm; MVD, 11.5 μm.

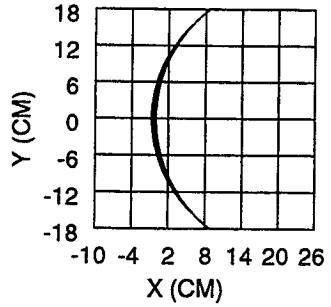

(iv) Sphere Diameter, 45.72 cm; MVD, 18.6 μm.

(a) Liquid water content, .2 gm/m^3; total temperature, -29.9° C.

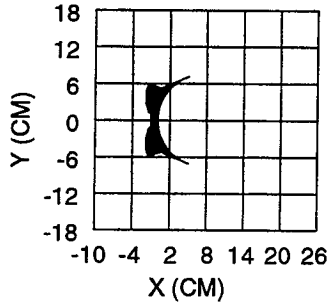

(i) Sphere Diameter, 15.04 cm; MVD, 11.5 μm.

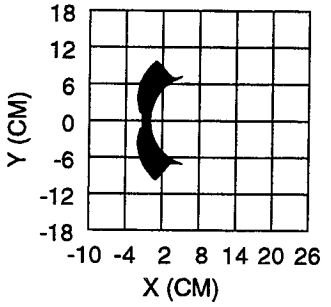

(ii) Sphere Diameter, 15.04 cm; MVD, 18.6 μm.

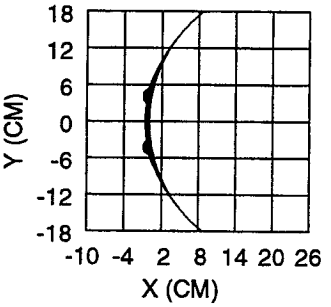

(iii) Sphere Diameter, 45.72 cm; MVD, 11.5 μm.

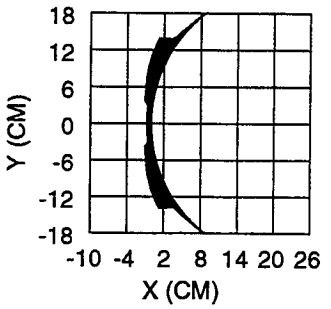

(iv) Sphere Diameter, 45.72 cm; MVD, 18.6 μm.

(b) Liquid water content, .695 gm/m^3; total temperature, -9.3° C.

Figure 14. - Theoretical ice shapes for a 45.72 cm and a 15.04 cm sphere. Icing conditions: Air-speed, 75 m/s; icing time, 30 minutes; static pressure 95840 Pa.

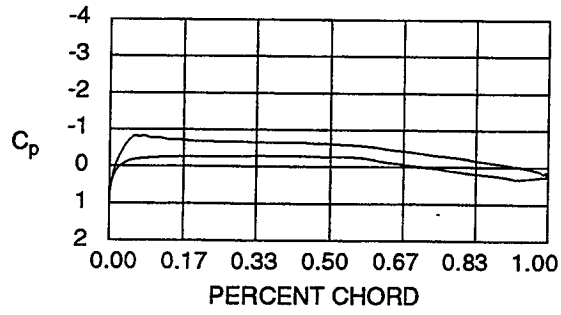

(a) AOA, 0°.

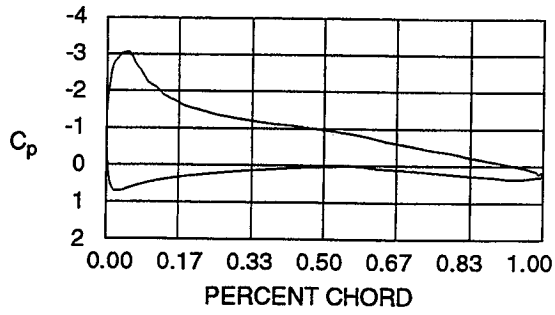

(b) AOA, 8°.

Figure 15. - Theoretical coefficient of pressure for the swept MS(1)-317 wing. Airspeed, 75 m/s; static temperature, 7° C; static pressure 95840 Pa.

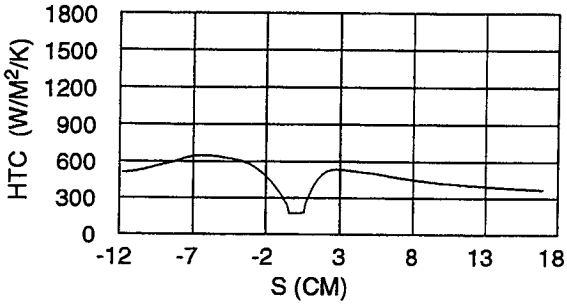

(a) AOA, 0°.

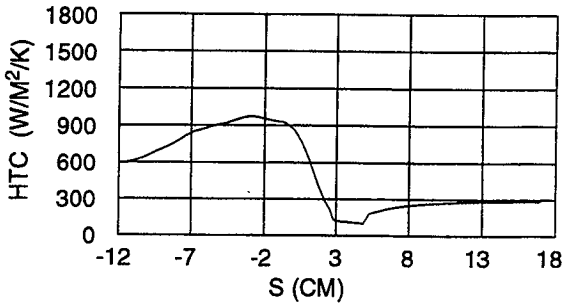

(b) AOA, 8°.

Figure 16. - Theoretical heat transfer for the swept MS(1)-317 wing. Airspeed, 75 m/s; static temperature, 7° C; static pressure 95840 Pa.

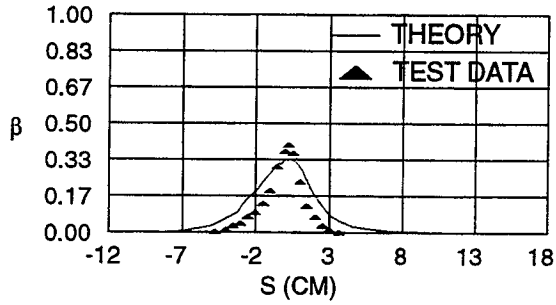

(a) AOA, 0°; MVD, 16 μm.

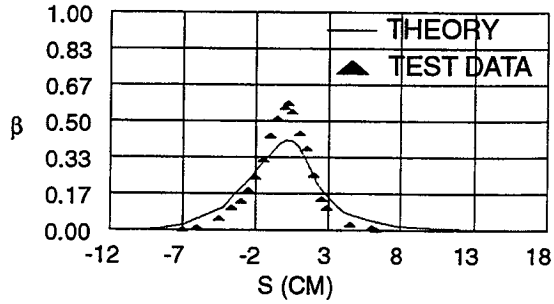

(b) AOA, 0°; MVD, 20 μm.

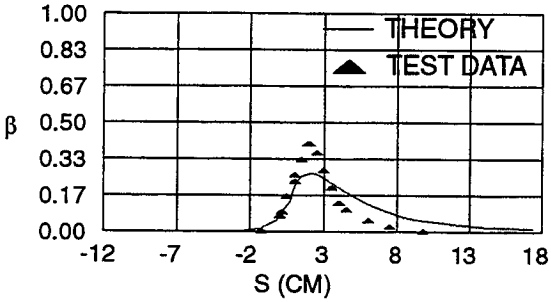

(c) AOA, 8°; MVD, 16 μm.

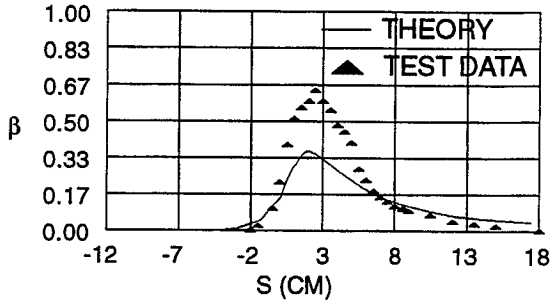

(d) AOA, 8°; MVD, 20 μm.

Figure 17. - Comparison of experimental and theoretical collection efficiency for the swept MS(1)-317 wing. Airspeed, 75 m/s; static temperature, 7° C; static pressure 95840 Pa.

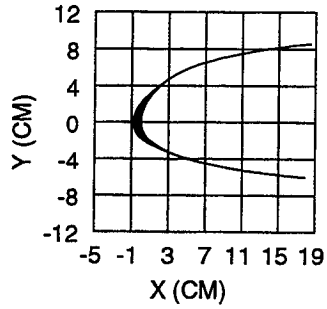

(i) AOA, 0°; MVD, 16 μm.

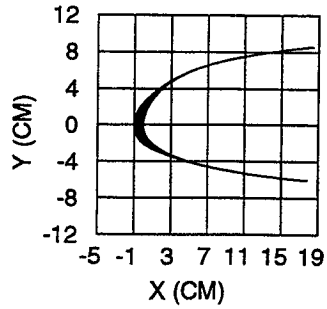

(ii) AOA, 0°; MVD, 20 μm.

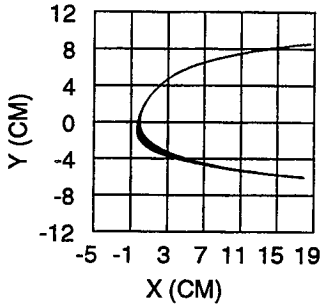

(iii) AOA, 0°; MVD, 16 μm.

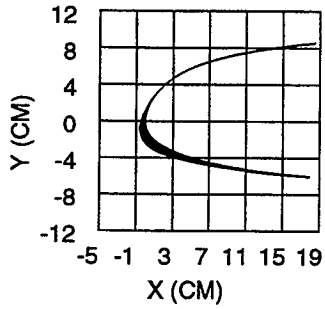

(iv) AOA, 0°; MVD, 20 μm.

(a) Liquid water content, .2 gm/m^3; total temperature -29.9° C.

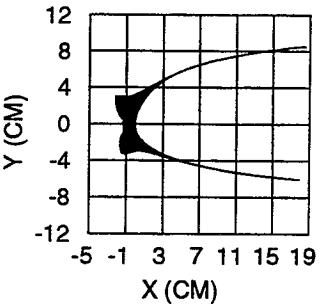

(i) AOA, 0°; MVD, 16 μm.

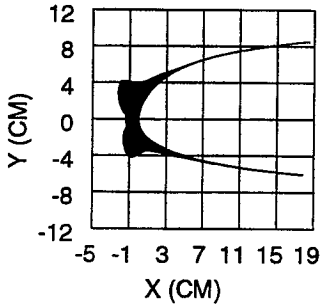

(ii) AOA, 0°; MVD, 20 μm.

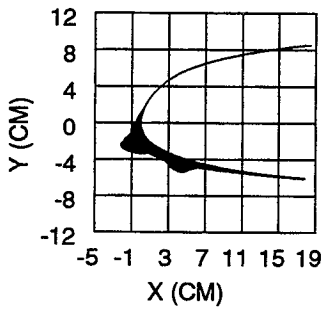

(iii) AOA, 8°; MVD, 16 μm.

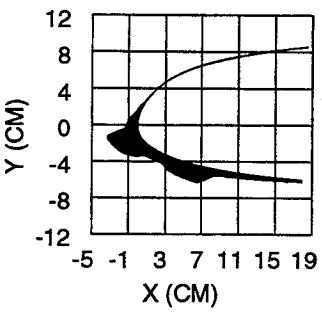

(iv) AOA, 8°; MVD, 20 μm.

(b) Liquid water content, .695 gm/m^3; total temperature -9.3° C.

Figure 18. - Theoretical ice shapes for the swept MS(1)-317 wing. Icing conditions: airspeed, 75 m/s; icing time, 30 minutes; static pressure 95840 Pa.

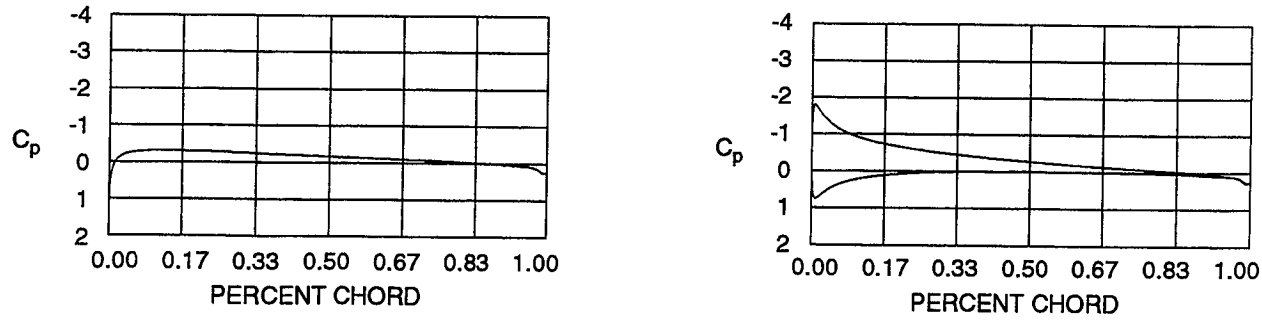

(a) AOA, 0°.

(b) AOA, 8°.

Figure 19. - Theoretical coefficient of pressure for the swept NACA-0012 wing tip. Airspeed, 75 m/s; static temperature, 7° C; static pressure 95840 Pa.

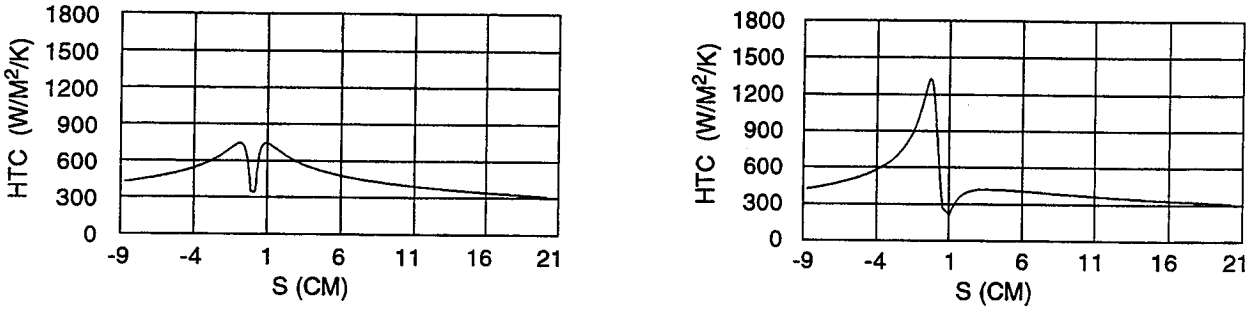

(a) AOA, 0°.

(b) AOA, 8°.

Figure 20. - Theoretical heat transfer coefficient for the swept NACA-0012 wing tip. Airspeed, 75 m/s; static temperature, 7° C; static pressure 95840 Pa.

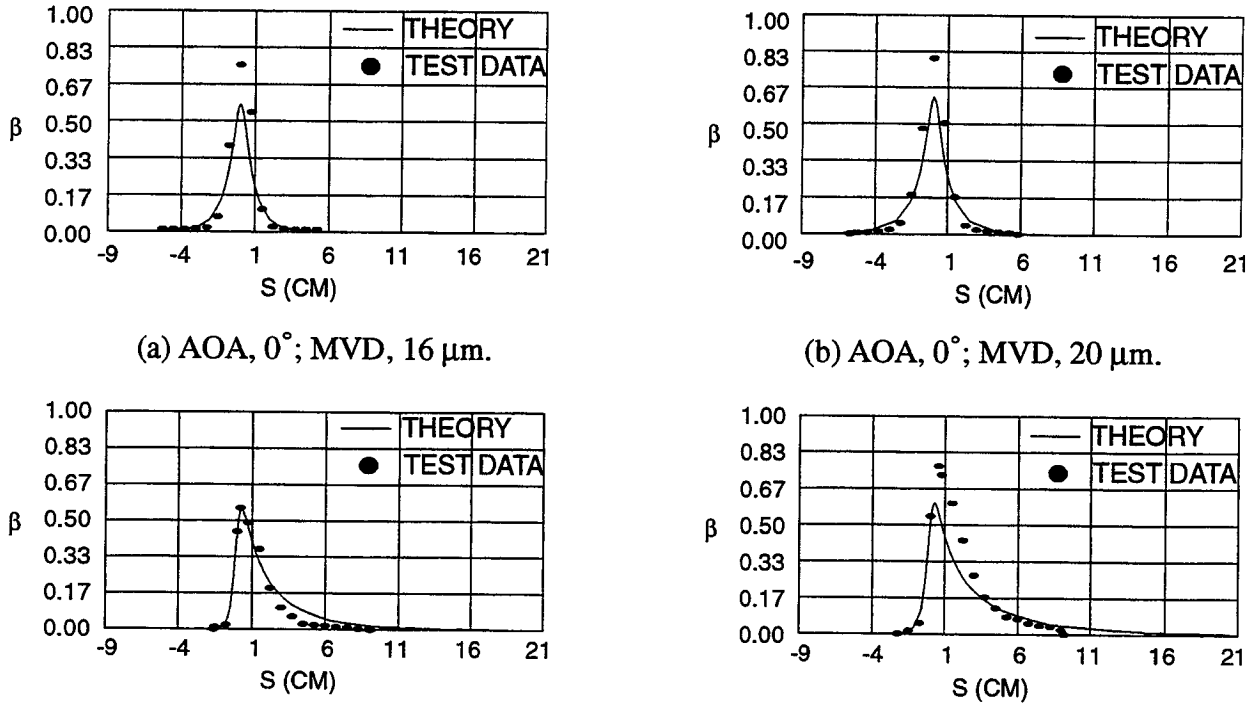

(a) AOA, 0°; MVD, 16 μm.

(b) AOA, 0°; MVD, 20 μm.

(c) AOA, 8°; MVD, 16 μm.

(d) AOA, 8°; MVD, 20 μm.

Figure 21. - Comparison of experimental and theoretical collection efficiency for the swept NACA-0012 wing tip. Airspeed, 75 m/s; static temperature, 7° C; static pressure 95840

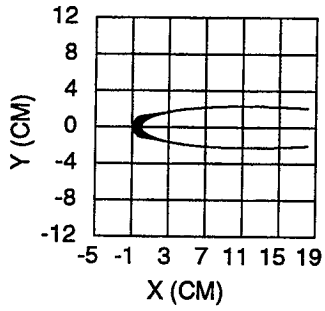

(i) AOA, 0°; MVD, 16 μm.

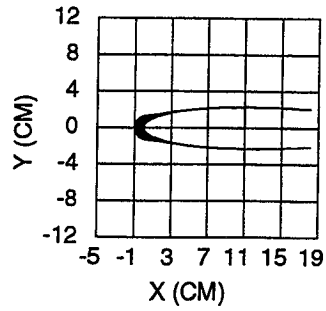

(ii) AOA, 0°; MVD, 20 μm.

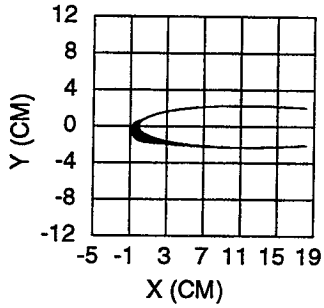

(iii) AOA, 0°; MVD, 16 μm.

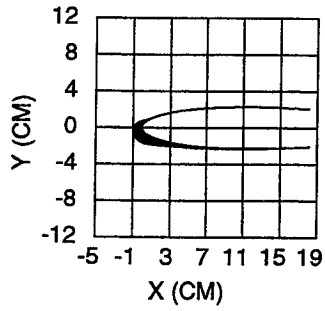

(iv) AOA, 0°; MVD, 20 μm.

(a) Liquid water content, .2 gm/m^3; total temperature -29.9° C.

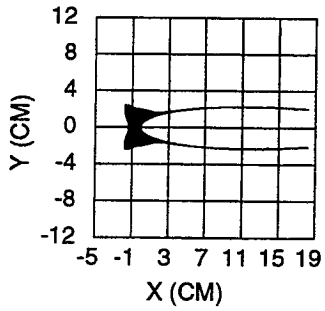

(i) AOA, 0°; MVD, 16 μm.

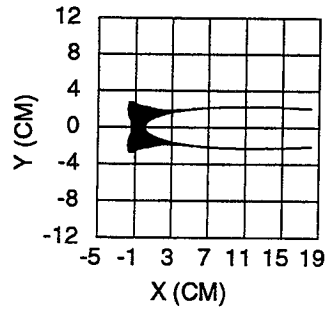

(ii) AOA, 0°;MVD, 20 μm.

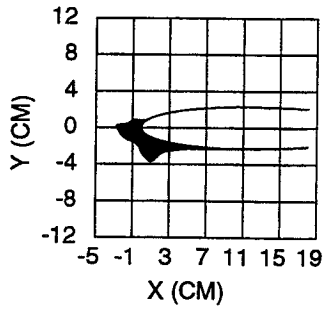

(iii) AOA, 8°; MVD, 16 μm.

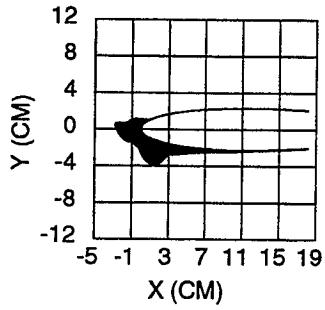

(iv) AOA, 8°; MVD, 20 μm.

(b) Liquid water content, .695 gm/m^3; total temperature -9.3° C.

Figure 22. - Theoretical ice shapes for the swept NACA-0012 wing tip. Icing conditions: airspeed, 75 m/s; icing time, 30 minutes; static pressure 95840 Pa.

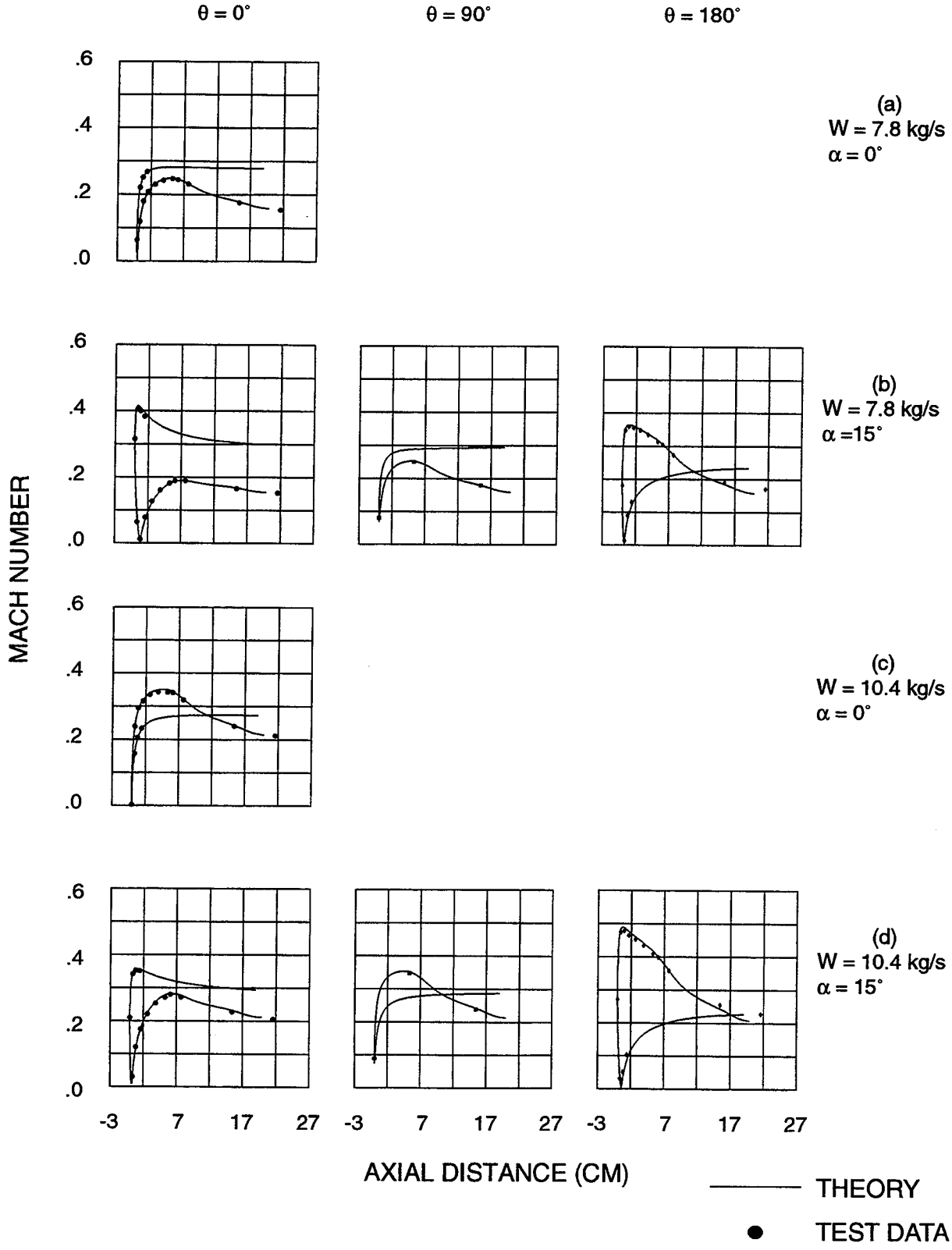

Figure 23. - Comparison of experimental and theoretical surface Mach numbers for the axisymetric inlet.

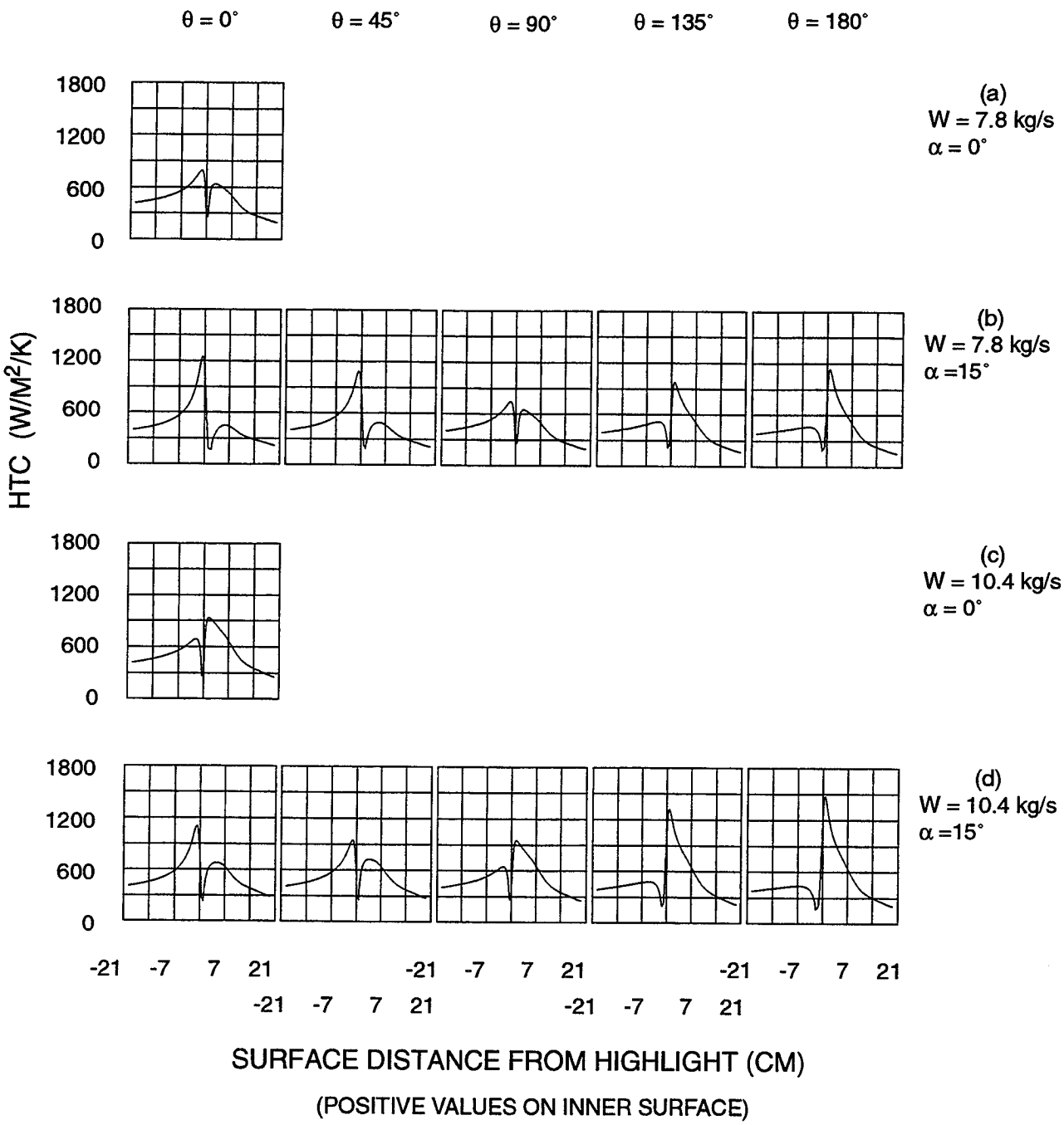

Figure 24. - Theoretical heat transfer distribution for the axisymetric inlet.

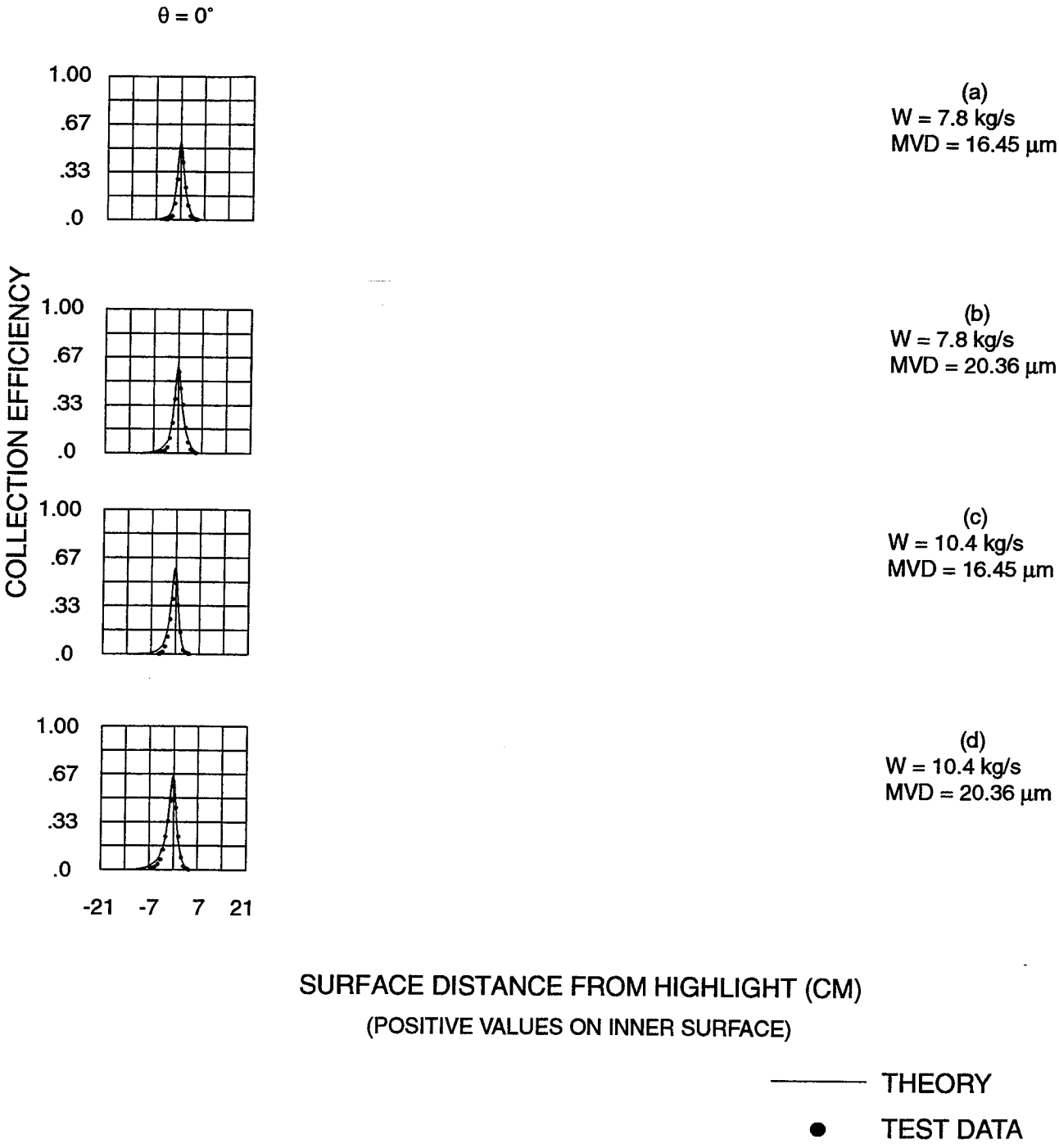

Figure 25. - Experimental and theoretical collection efficiency for the axisymetric inlet for $\alpha = 0°$. Airspeed, 75 m/s; static temperature, 7° C; static pressure 95840 Pa.

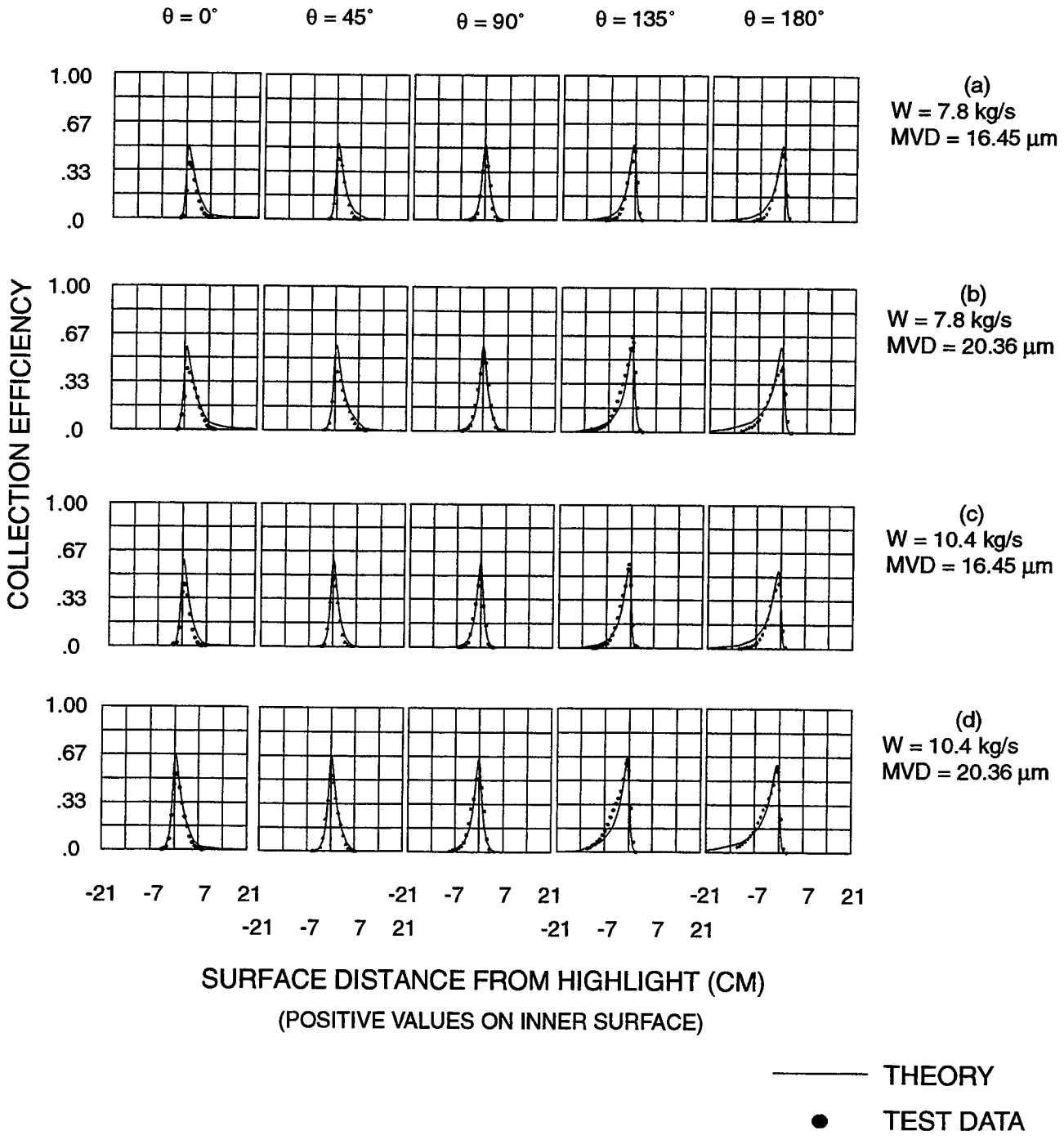

Figure 26. - Experimental and theoretical collection efficiency for the axisymetric inlet for α = 15°. Airspeed, 75 m/s; static temperature, 7° C; static pressure 95840 Pa.

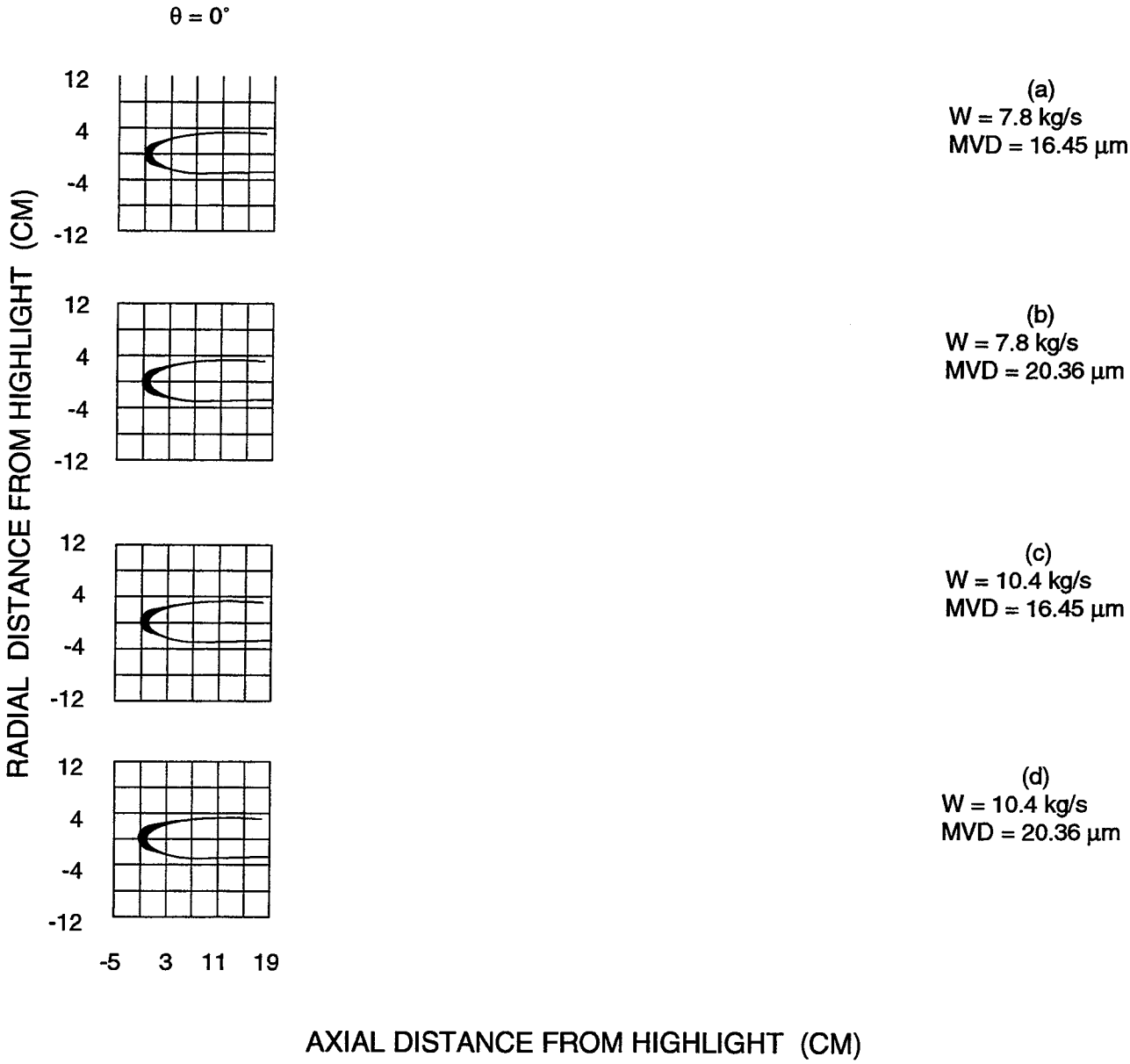

Figure 27. - Theoretical ice shapes for the axisymetric inlet for $\alpha = 0^\circ$. Icing conditions: airspeed, 75 m/s; icing time, 30 minutes; static temperature, -29.9° C, liquid water content, .2 g/ m3.

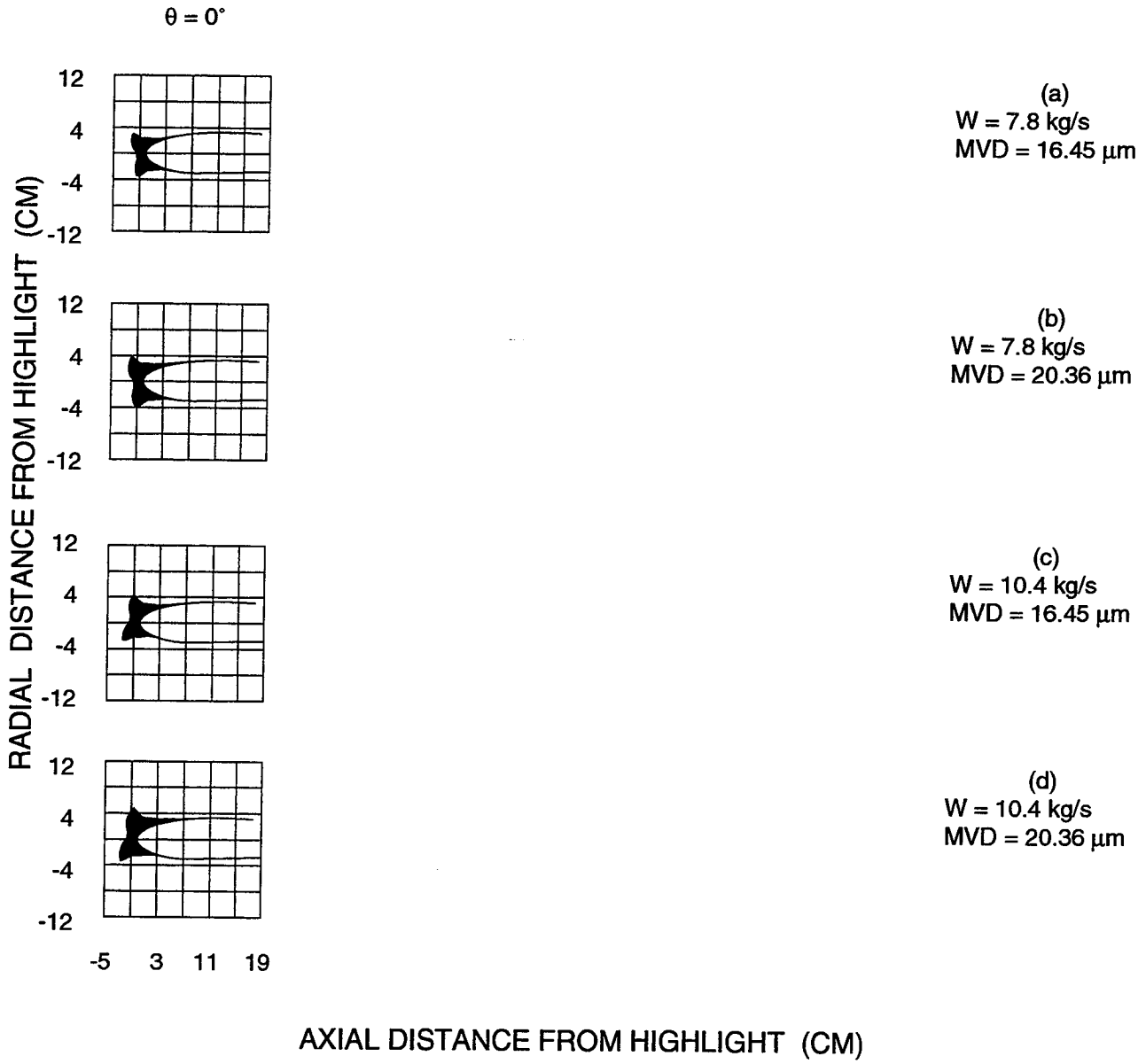

Figure 28. - Theoretical ice shapes for the axisymetric inlet for $\alpha = 0^{\circ}$. Icing conditions: airspeed, 75 m/s; icing time, 30 minutes; static temperature, -9.3° C, liquid water content, .695 g/ m3.

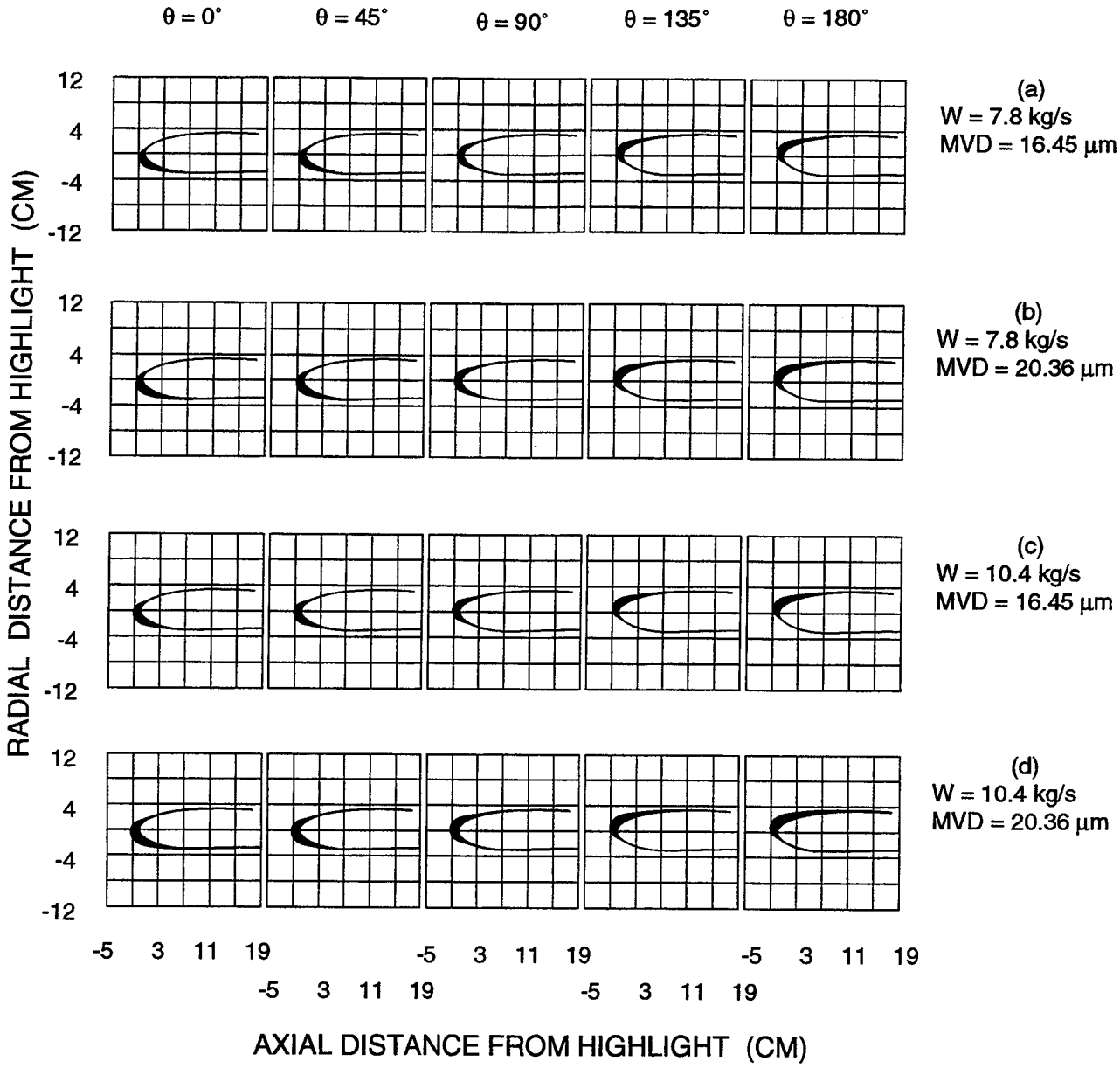

Figure 29. - Theoretical ice shapes for the axisymetric inlet for $\alpha = 15^{\circ}$. Icing conditions: air-speed, 75 m/s; icing time, 30 minutes; static temperature, -29.9° C, liquid water content, .2 g/m3.

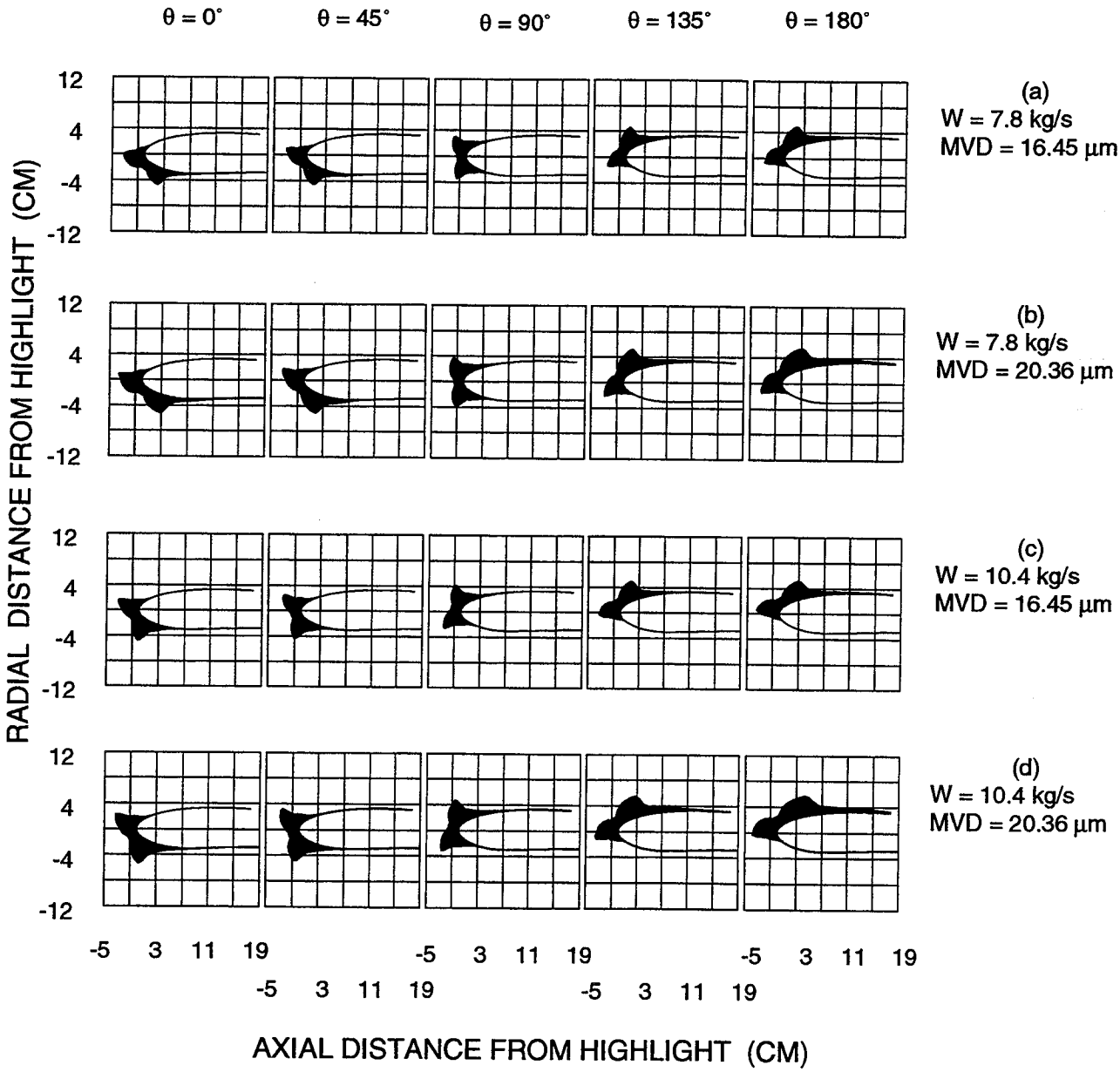

Figure 30. - Theoretical ice shapes for the axisymetric inlet for $\alpha = 15^{\circ}$. Icing conditions: air-speed, 75 m/s; icing time, 30 minutes; static temperature, -9.3° C, liquid water content, .695 g/m3.

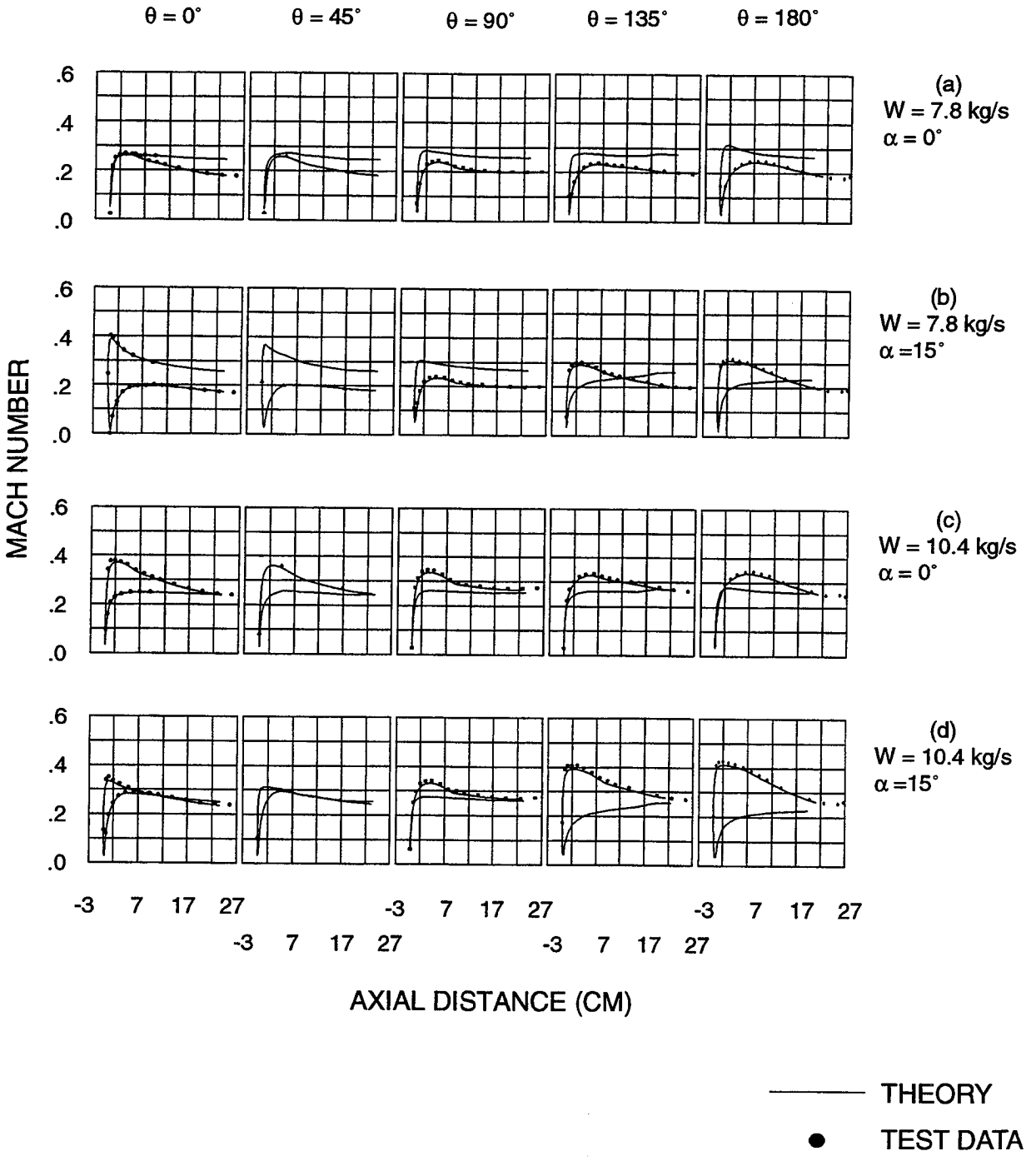

Figure 31. - Comparison of experimental and theoretical surface Mach numbers for the Boeing 737-300 inlet.

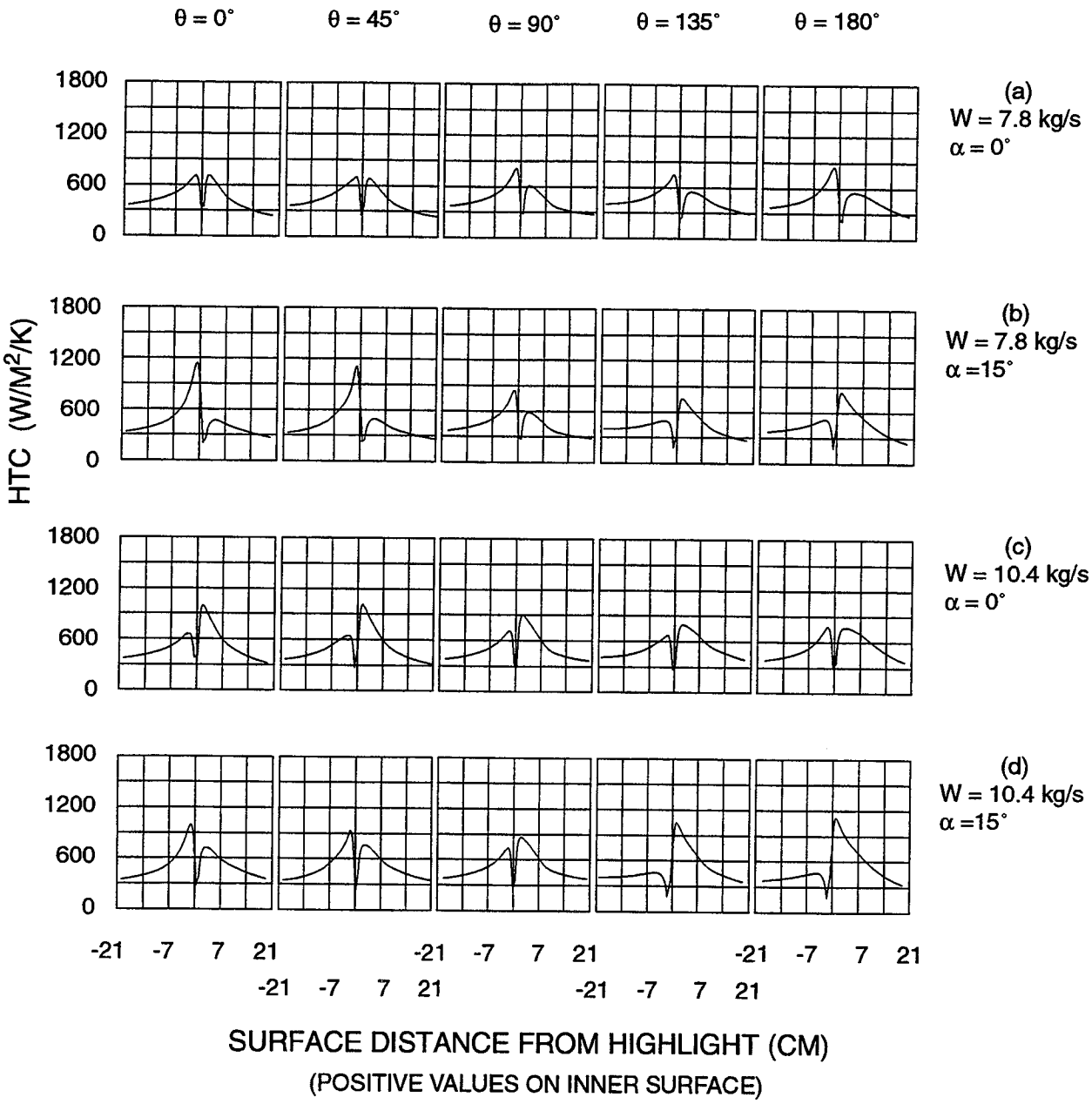

Figure 32 - Theoretical heat transfer distribution for the Boeing 737-300 inlet.

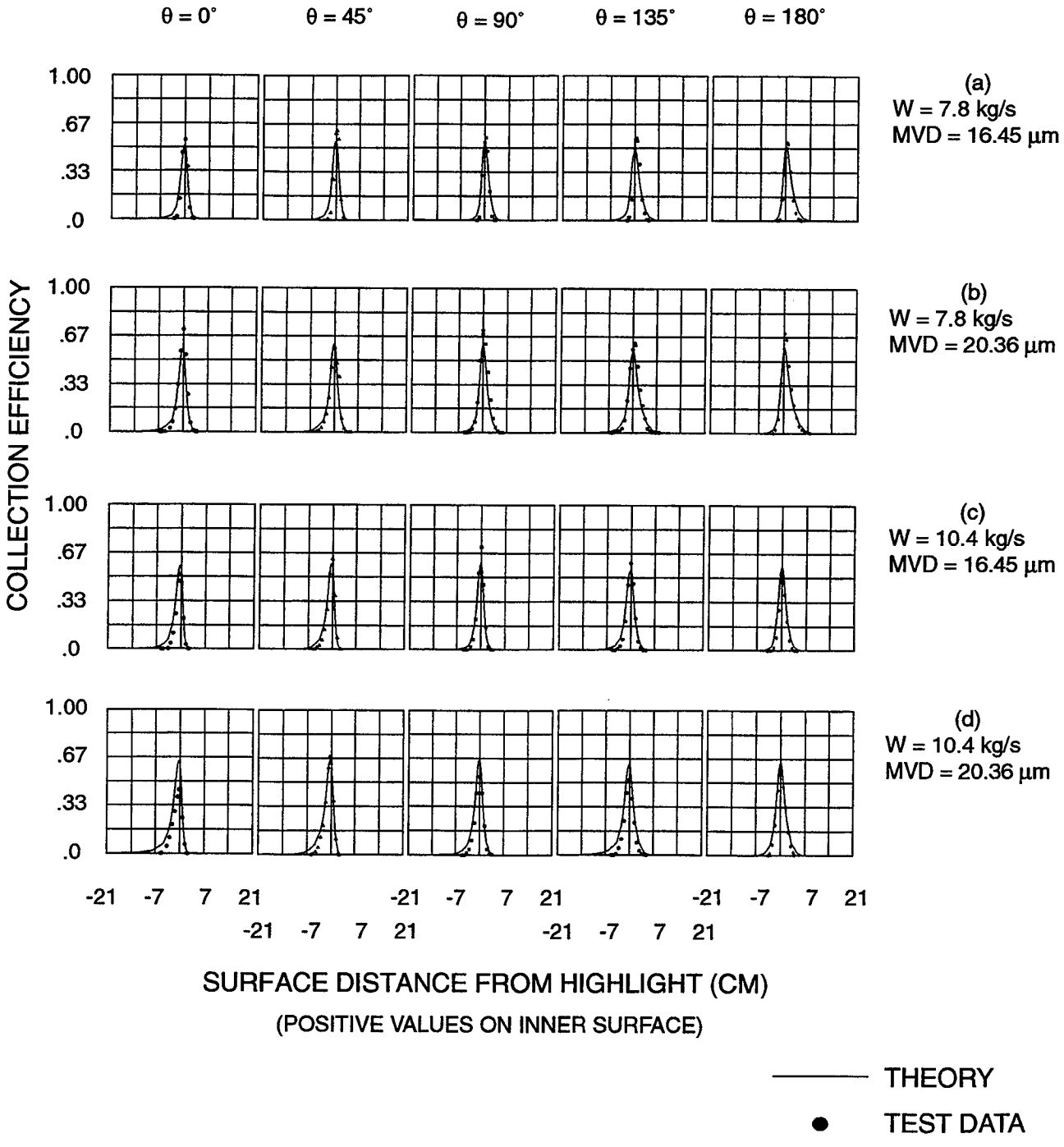

Figure 33. - Experimental and theoretical collection efficiency for the Boeing 737-300 inlet for α = 0°. Airspeed, 75 m/s; static temperature, 7° C; static pressure 95840 Pa.

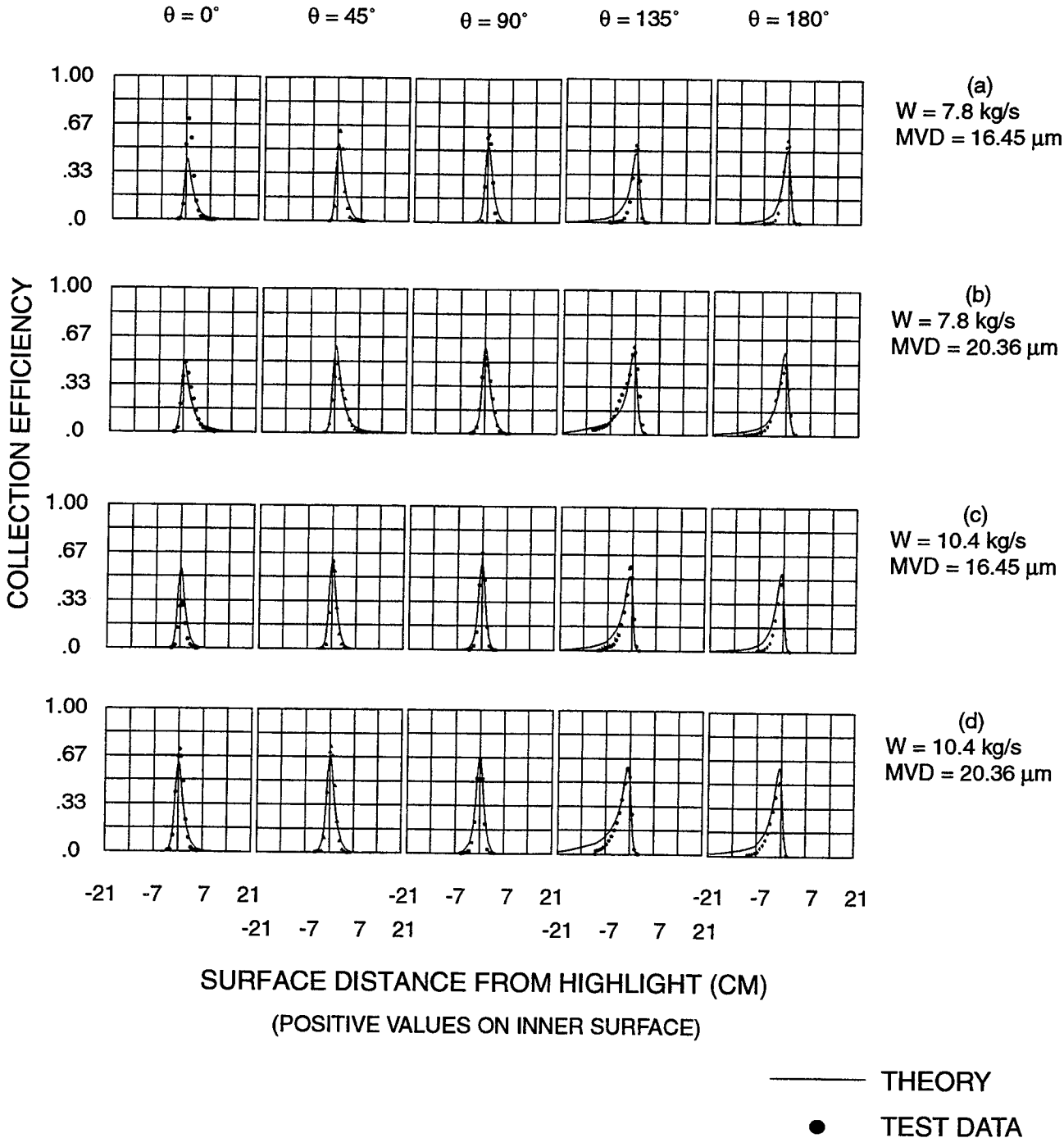

Figure 34. - Experimental and theoretical collection efficiency for the Boeing 737-300 inlet for α = 15°. Airspeed, 75 m/s; static temperature, 7° C; static pressure 95840 Pa.

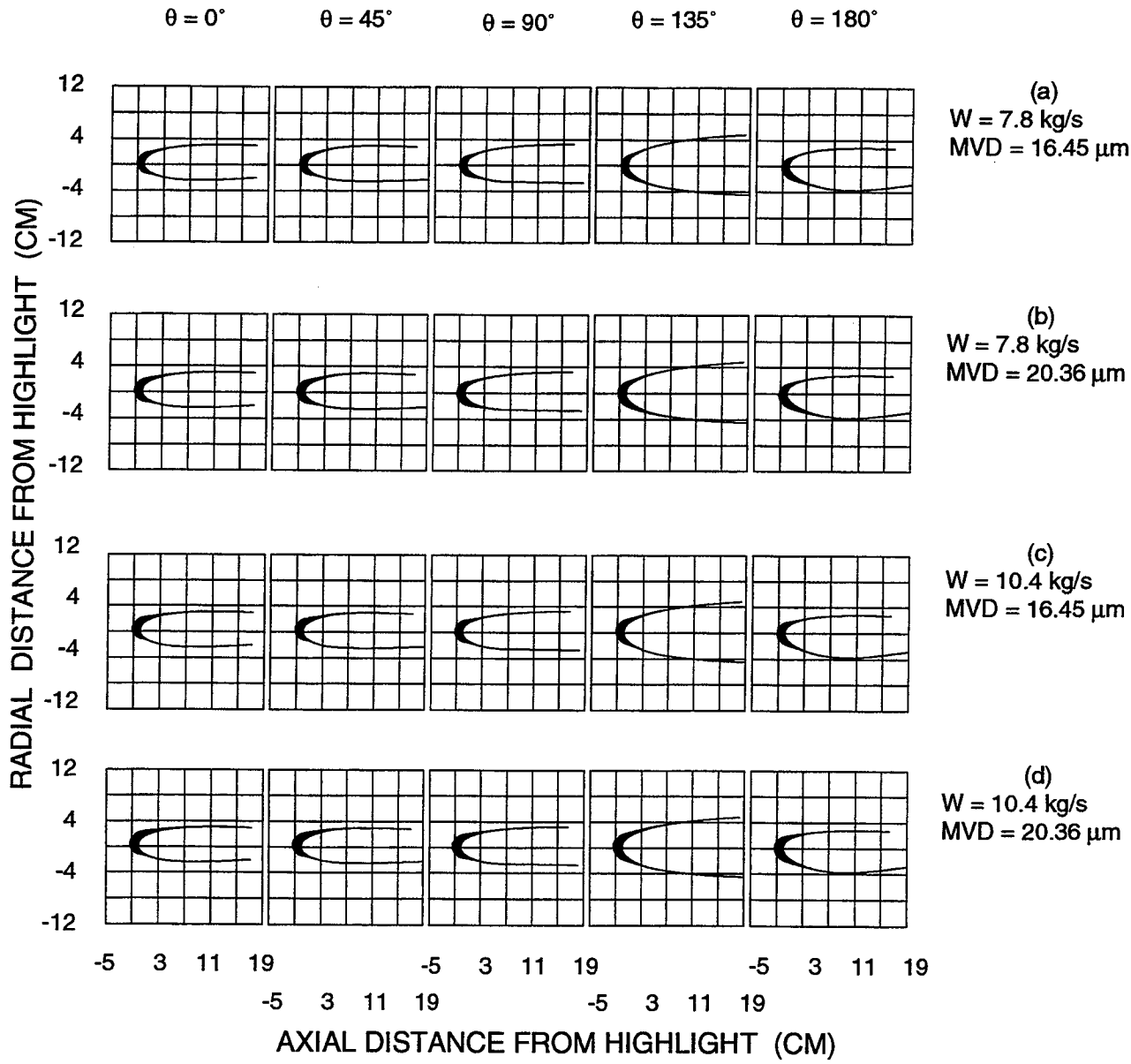

Figure 35. - Theoretical ice shapes for the Boeing 737-300 inlet for $\alpha = 0^\circ$. Icing conditions: air-speed, 75 m/s; icing time, 30 minutes; static temperature, -29.9° C, liquid water content, .2 g/m3.

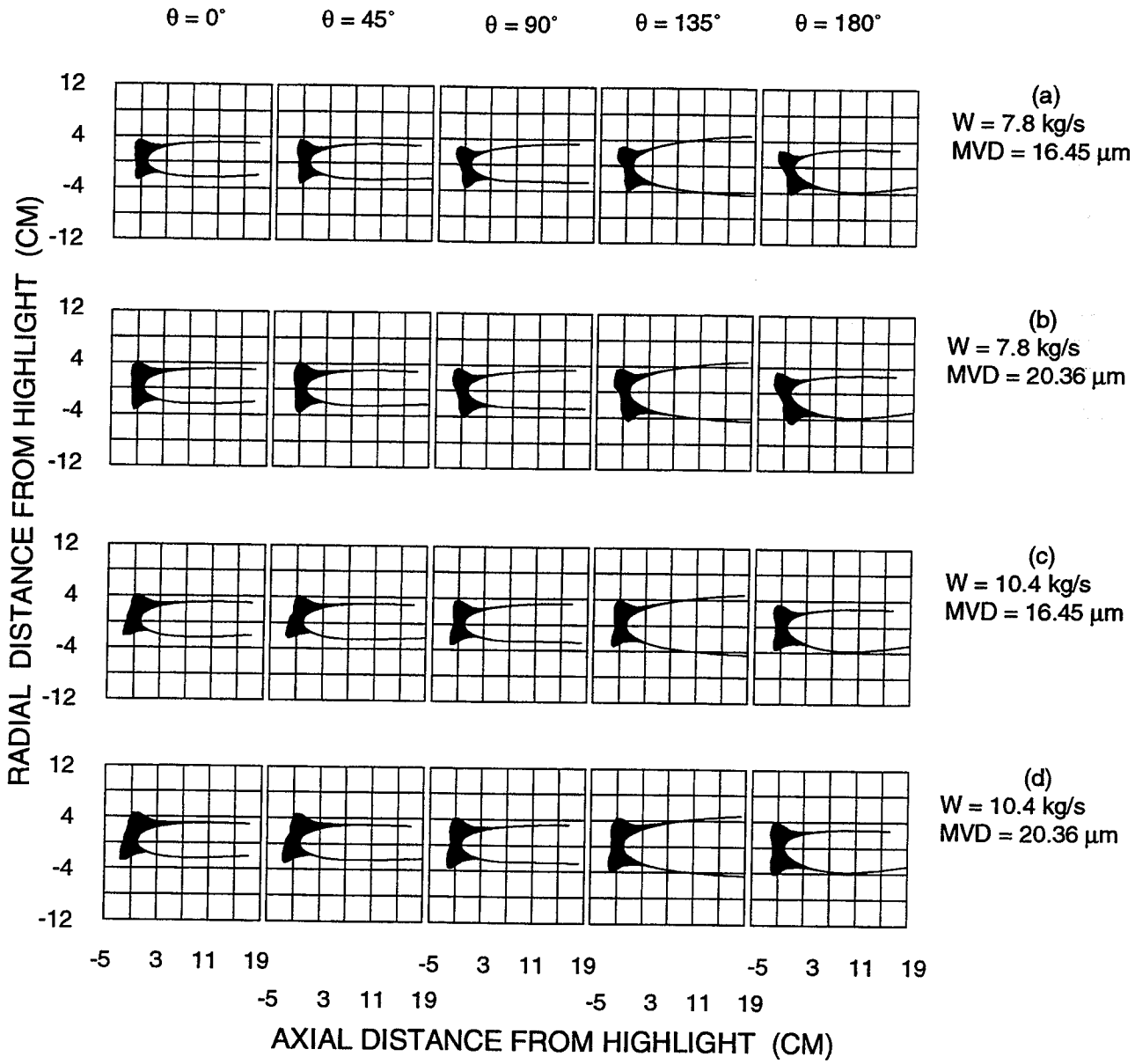

Figure 36 - Theoretical ice shapes for the Boeing 737-300 inlet for $\alpha = 0^{\circ}$. Icing conditions: air-speed, 75 m/s; icing time, 30 minutes; static temperature, -9.3° C, liquid water content, .695 g/m3.

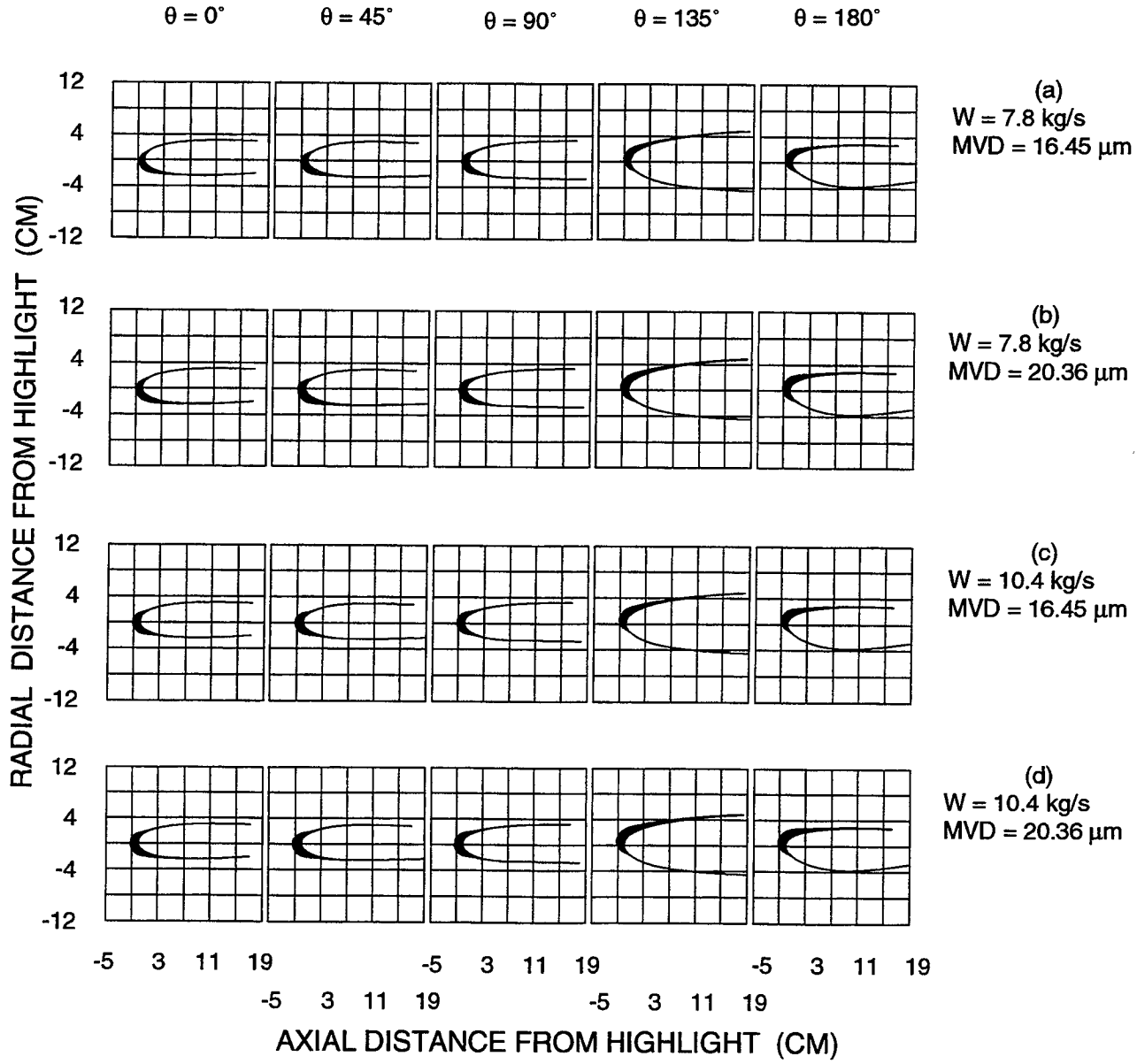

Figure 37. - Theoretical ice shapes for the Boeing 737-300 inlet for $\alpha = 15^{\circ}$. Icing conditions: airspeed, 75 m/s; icing time, 30 minutes; static temperature, -29.9° C, liquid water content, .2 g/m3.

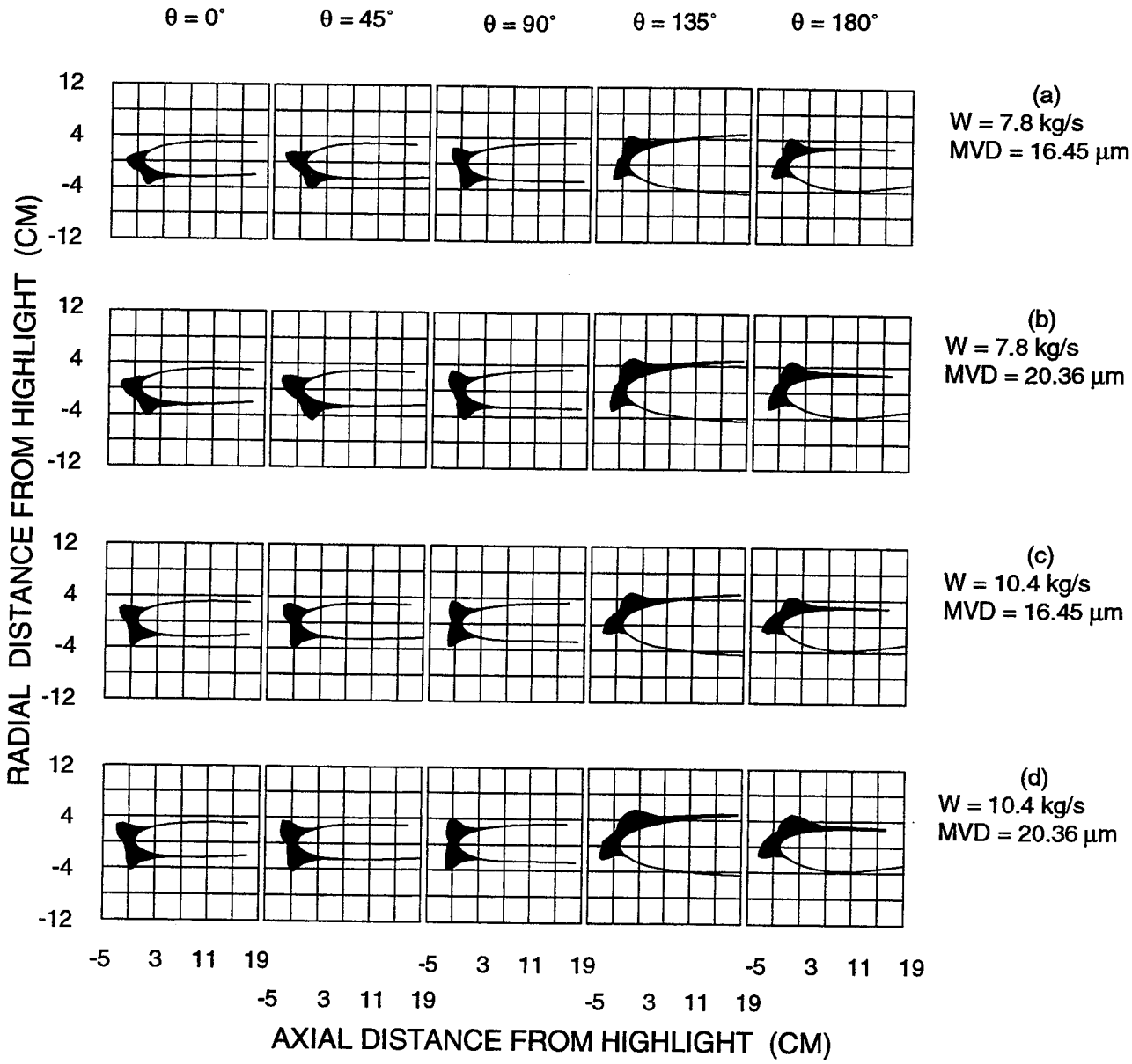

Figure 38 - Theoretical ice shapes for the Boeing 737-300 inlet for $\alpha = 15^{\circ}$. Icing conditions: air-speed, 75 m/s; icing time, 30 minutes; static temperature, -9.3° C, liquid water content, .695 g/m3.

REPORT DOCUMENTATION PAGE

Form Approved
OMB No. 0704-0188

1. AGENCY USE ONLY (*Leave blank*)	2. REPORT DATE	3. REPORT TYPE AND DATES COVERED
	January 1995	Technical Memorandum

4. TITLE AND SUBTITLE

Collection Efficiency and Ice Accretion Calculations for a Sphere, a Swept MS(1)-317 Wing, a Swept NACA-0012 Wing Tip, an Axisymmetric Inlet, and a Boeing 737-300 Inlet

5. FUNDING NUMBERS

WU–505–68–10

6. AUTHOR(S)

C.S. Bidwell and S.R. Mohler, Jr.

7. PERFORMING ORGANIZATION NAME(S) AND ADDRESS(ES)

National Aeronautics and Space Administration
Lewis Research Center
Cleveland, Ohio 44135–3191

8. PERFORMING ORGANIZATION REPORT NUMBER

E–9381

9. SPONSORING/MONITORING AGENCY NAME(S) AND ADDRESS(ES)

National Aeronautics and Space Administration
Washington, D.C. 20546–0001

10. SPONSORING/MONITORING AGENCY REPORT NUMBER

NASA TM–106831
AIAA–95–0755

11. SUPPLEMENTARY NOTES

Prepared for the 33rd Aerospace Sciences Meeting and Exhibit sponsored by the American Institute of Aeronautics and Astronautics, Reno, Nevada, January 9–12, 1995. C.S. Bidwell, NASA Lewis Research Center, and S.R. Mohler, Jr., NYMA, Inc., Engineering Services Division, 2001 Aerospace Parkway, Brook Park, Ohio 44142 (work funded by NASA Contract NAS3–27186). Responsible person, C.S. Bidwell, organization code 2720, (216) 433–3947.

12a. DISTRIBUTION/AVAILABILITY STATEMENT

Unclassified - Unlimited
Subject Categories 02 and 03

This publication is available from the NASA Center for Aerospace Information, (301) 621–0390.

12b. DISTRIBUTION CODE

13. ABSTRACT (*Maximum 200 words*)

Collection efficiency and ice accretion calculations have been made for a sphere, a swept MS(1)-317 wing, a swept NACA-0012 wing tip, an axisymmetric inlet, and a Boeing 737-300 inlet using the NPARC flow solver and the NASA Lewis LEWICE3D grid based ice accretion code. Euler flow solutions for the geometries were generated using the NPARC flow solver. The LEWICE3D grid based ice accretion program was used to calculate the impingement efficiencies and ice shapes. Ice shapes typifying rime and mixed icing conditions were generated for a 30 minute hold condition. All calculations were performed on an SGI Model Power Challenge Computer. The results have been compared to experimental flow and impingement data. In general, the calculated flow and collection efficiencies compared well with experiment, and the ice shapes looked reasonable and appeared representative of the rime and mixed icing conditions for which they were calculated.

14. SUBJECT TERMS

Trajectory code validation; Water droplet trajectories; Trajectory codes; Impingement characteristics; Ice accretion codes; Ice accretion characteristics; Aircraft icing; Inlet ice accretion prediction

15. NUMBER OF PAGES

45

16. PRICE CODE

A03

17. SECURITY CLASSIFICATION OF REPORT	18. SECURITY CLASSIFICATION OF THIS PAGE	19. SECURITY CLASSIFICATION OF ABSTRACT	20. LIMITATION OF ABSTRACT
Unclassified	Unclassified	Unclassified	